Using Stream Gages to Represent Antecedent Moisture Conditions in the Antecedent Moisture Model

Alex R. Luedke

Civil and Architectural Engineering and Construction Management Department

Milwaukee School of Engineering

Author Note

Alexander Luedke, Civil and Architectural Engineering and Construction Management Department, Milwaukee School of Engineering.

A report submitted to the faculty of the Milwaukee School of Engineering in partial fulfillment of the requirements for the degree of Master of Science in Civil Engineering, May 2023.

Correspondence concerning this paper should be addressed to Alex R. Luedke, 1025 N. Broadway, Milwaukee, WI 53202. Email: luedkea@msoe.edu

Abstract

When modeling wet weather flow in sanitary sewers the RTK method is often used. The RTK method converts a specified amount of rainfall into sewer flow, regardless of changes in the soil's moisture content and saturation. Robert Czachorski and Tobin VanPelt (2001) sought to remedy this issue when they developed the antecedent moisture modeling (AMM) procedure, which explicitly accounts for antecedent moisture conditions. AMM tracks antecedent moisture using rain and temperature signals. The rain signal adds moisture to the soil according to the magnitude of the temperature signal. High temperatures reduce added soil moisture because evaporation and transpiration are higher, resulting in drier antecedent moisture conditions, while low temperatures do the reverse. Since 2021, AMM has been applied with great success on hundreds of projects (Edgren et al., 2023). AMM, in its current form as documented by Czachorski, Edgren and Gonwa (2023), has the potential to revolutionize sanitary sewer system hydrologic modeling. Nearby streams experience roughly the same antecedent moisture conditions as a sanitary sewer system. Is it possible that streamflow provides a better indicator signal of antecedent moisture conditions than temperature? The purpose of this paper is to explain an investigation with a focus on determining if streamflow provides a better indicator of antecedent moisture conditions than temperature. AMM using temperature was compared against AMM using streamflow, and the models were calibrated using a Bayesian Optimization algorithm. The results indicated that streamflow produces a comparable or better representation of antecedent moisture conditions. Out of the various streamflow methods, two-level models utilizing a large regional stream produced the lowest error. Future studies investigating streamflow's ability to represent antecedent moisture should include a larger sample size of sewer systems in order to validate these results.

Keywords: antecedent moisture, antecedent moisture model, wet weather flow, rainfall derived inflow / infiltration [RDI/I], sanitary sewers, streamflow

Table of Contents

List of Figures

List of Tables

Using Stream Gages to Represent Antecedent Moisture Conditions in the Antecedent Moisture Model

Sewer systems have been crucial in human civilization for thousands of years, with the earliest dating back to the Mesopotamian Empire in Iraq (ca. 4000 BC) (De Feo et al., 2014). At that time, sewer systems were nothing more than a crude drain positioned next to a street and have only become increasingly complex as time marches forward (De Feo et al., 2014). Sewer systems in the United States (US) have been constructed over a long period of time (Lai, 2008). The increasing age of sewers has been a concern of governmental agencies and various institutions in the US. A study conducted by the American Society of Civil Engineers (Black & Veatch, 1999) analyzed the ages of the sewers in the collection system of 42 wastewater utilities across the US. The wastewater utilities included in the study ranged in age from 117 years old to new with the average age of sewers being 33 years (Black & Veatch, 1999). The distribution of the sewers' ages was analyzed in the study, which found that 18.2% of sewers were 0 to 10 years old, 22.8% were 11 to 20 years old, 41.1% were 21 to 50 years old, 16.4% were 51 to 100 years old, and 1.6% were greater than 100 years old. Since that study took place 24 years ago, the average age is surely much higher now. Lai (2008) states, "Older sewers were constructed mainly of vitrified clay, brick, and concrete, while modern sewers were constructed of plastic, ductile iron, steel, and reinforced concrete" (p. 1).

Older sewers constructed of clay, brick, and concrete are more susceptible to deterioration than modern sewers (Lai, 2008). Over time, deterioration causes cracks and openings in the sewer's structure, allowing extraneous water sources to enter the system. Intrusive water that invades sewer systems is referred to as rainfall derived inflow / infiltration (RDI/I) and it causes increased flows in sanitary sewer systems. RDI/I can be introduced to the

system from various sources, including stormwater, meltwater, and groundwater. When a sewer experiences increased flow conditions as a result of RDI/I, the sewer is considered to be in a period of a wet weather flow (WWF). WWF is difficult to model, predict, quantify, and control. Hydrologic models that are able to accurately relate the quantity of rainfall to WWF are imperative in the design of strategies that limit the environmental and public health impacts of excessive sanitary sewer system WWF.

Currently the US Environmental Protection Agency (US EPA) encourages the use of the RTK method for modeling WWF based on a review of available WWF prediction methods in sanitary sewers (Lai, 2008). The RTK method has since been implemented in the EPA's Storm Water Management Model (SWWM), which is used frequently in the field of hydrology. The RTK method assumes a constant capture fraction, meaning that a constant percentage of rainfall volume is converted to RDI/I (Walski, 2021). However, a constant capture fraction does not accurately represent reality. The capture fraction of a given catchment area fluctuates during WWF periods, increasing with the system's moisture conditions. These fluctuations are not considered by this method, but instead, its parameters are changed depending on the time of year. Parameters are typically designated by month, increasing the number of calibratable parameters by up to a factor of twelve. While helpful, monthly parameters do not address short term fluctuations in a system's capture fraction during an RDI/I event. Depending on the antecedent moisture conditions, the volume of RDI/I response experienced by a sewer system can increase by orders of magnitude, requiring a hydrologic modeling method that continuously incorporates continuously varying antecedent moisture (W. Gonwa, personal communication, March 17, 2023).

The difficulty of modeling WWF in sanitary sewers lies in accurately representing the antecedent moisture conditions of a sewer's catchment area. In an effort to address this, Robert Czachorski and Tobin Van Pelt (2002) developed a model with the ability to track and predict antecedent moisture conditions and seasonal effects, aptly naming the procedure antecedent moisture modeling (AMM). AMM utilizes rainfall and temperature signals to track the antecedent moisture conditions of the catchment area in question. The rain signal adds moisture to the system while the temperature signal determines the magnitude of the rain signal. High temperatures reduce added soil moisture due to evaporation and transpiration being higher, while low temperatures increase added soil moisture for the opposite reason. AMM's ability to actively track the hydrologic conditions of a catchment area allows it to continuously model sewer flow over a long period of time, unlike some other RDI/I methods, which are event based (i.e., they model on a storm-by-storm basis). Since its creation, AMM has been utilized in hundreds of projects and has demonstrated its ability to accurately simulate antecedent moisture dynamics (Edgren et al., 2023).

While the rainfall signal in AMM is a direct measure of the rainfall volume falling over the catchment area, the temperature signal is an indirect measure of the evaporation, transpiration, and soil moisture. Is it possible that streamflow could be a more accurate indicator signal of antecedent moisture conditions than temperature in AMM? Streams are directly impacted by antecedent moisture conditions and experience roughly the same antecedent moisture conditions as nearby sanitary sewer systems. Additionally, streamflow data have been collected for decades by the United States Geological Survey (USGS) scientific agency and other federal, state, and local agencies making it widely available over long periods of time (W. Gonwa, personal communication, May 16, 2022). If streamflow were used in place of

temperature, what method of implementing streamflow in AMM is the most proficient? This paper seeks to provide the answers to these questions through an exploration of streamflow as an indicator of antecedent moisture conditions in AMM.

Background

To better understand the data, concepts, and nomenclature being used in regard to the implementation of streamflow in AMM, additional questions must be answered. What is the difference between a sanitary sewer and a combined sewer? What causes RDI/I, and what is it comprised of? What is antecedent moisture, and what are its effects on RDI/I? What components make up sanitary sewer flow? What are hydrographs, and what information can we derive from them? How is the AMM procedure structured, and what are its underlying equations? How will streamflow be implemented into AMM? Which streams and sewers will be analyzed in this study? What is Bayesian optimization and how was it used to assist in model calibration? The answers to these questions will prepare the reader for the methodology and results sections, in which the following concepts will be utilized to implement streamflow into AMM and analyze its proficiency compared to temperature based antecedent moisture models.

Sanitary Sewers and Combined Sewers

A literature review by the Office of Water Programs at the California State University Sacramento (Office of Water Programs, 2008) states “There are two types of public sewer systems used in the United States for collecting and conveying sanitary sewage, combined sewer systems and sanitary sewer systems” (p. 1). Combined sewer systems collect stormwater runoff through street drains and other stormwater inflow locations while simultaneously collecting wastewater flows from commercial, residential, and public structures. Sanitary sewer systems only collect the wastewater portion of flows along their flow route. Because sanitary sewer

systems only collect wastewater flows, they are usually paired with stormwater sewers, which are designed specifically for conveying stormwater runoff. When a sanitary sewer and stormwater sewer are utilized in tandem, it is commonly referred to as a separated sewer system (Village of Shorewood, WI, 2009). Figure 1 displays a diagram of a typical separated sewer system.

Figure 1

Diagram of Typical Separated Sewer System in Shorewood, WI

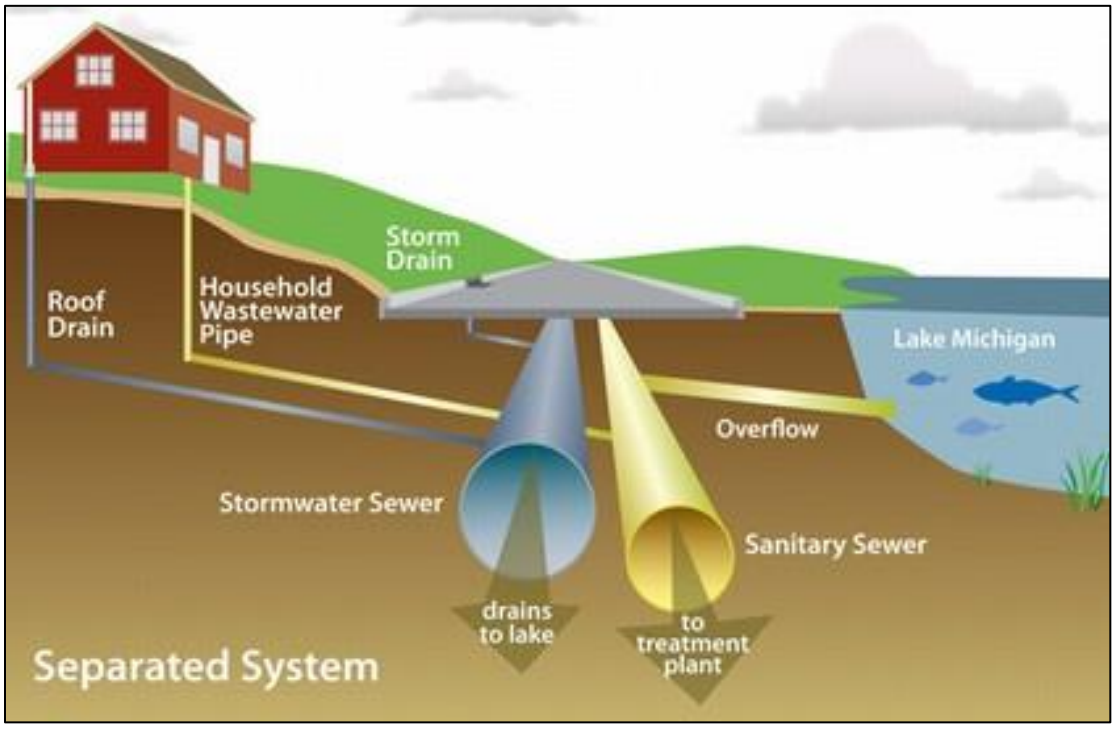

Note. Adapted from "Sanitary Sewer Systems", by Village of Shorewood, Wisconsin, 2009, para.1 (https://www.villageofshorewood.org/884/Sanitary-Sewer-System).

This paper focuses only on sanitary sewer systems because antecedent moisture is a much more important factor in sanitary sewer WWF than in combined sewers.

Rainfall Derived Inflow / Infiltration

Rainfall derived inflow / infiltration, commonly referred to as I/I and RDI/I, is made up of two components. The first is inflow, which accounts for open pathways allowing water into the sanitary sewer such as roof drain connections, uncapped cleanouts, and faulty manhole covers (WEF Collection Systems Committee, 2017). Some components of inflow are allowed by local ordinances, such as preordinance foundation drain connections that tie directly into the sanitary sewer.

The second component of RDI/I is infiltration. Infiltration in RDI/I consists of stormwater that infiltrates into the ground and enters a sanitary sewer system through cracks, faulty lateral connections, or root intrusions (WEF Collection Systems Committee, 2017). Figure 2 contains a diagram depicting the various routes that RDI/I's inflow and infiltration components can take to enter sewers. Older sewer systems in need of rehabilitation experience large quantities of rainfall induced infiltration due to their outdated materials and construction methods (Lai, 2008). Vitrified clay, a common material used in older sewers, is brittle in tension and prone to developing cracks over time, allowing large quantities of rain induced infiltration into sanitary sewers (Lai, 2008).

Figure 2

Typical Sources of RDI/I in Sanitary Sewer Systems

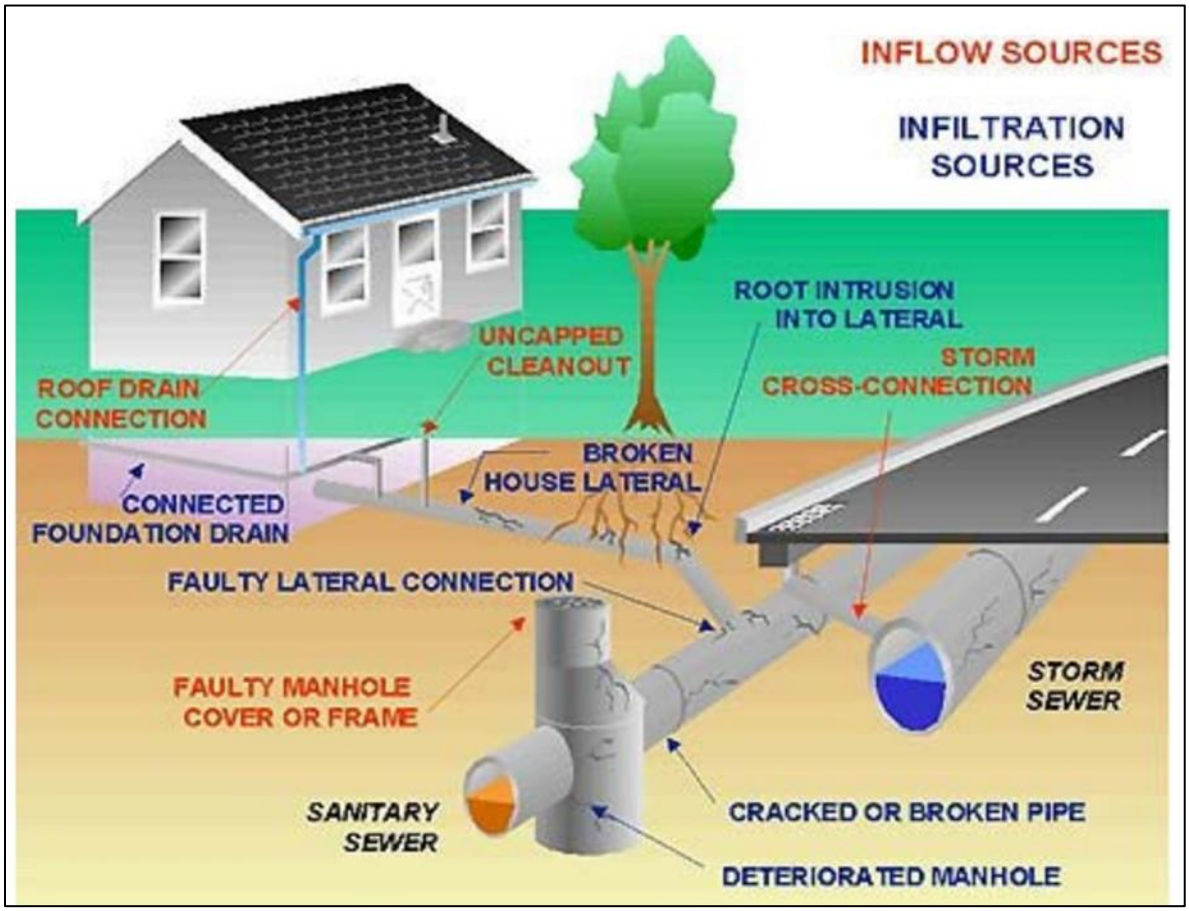

Note. Adapted from Sanitary Sewer Systems: Rainfall Derived Infiltration and Inflow (RDI/I) Modeling Fact Sheet, 2017, p. 1 (https://www.wef.org/globalassets/assets-wef/direct-download-library/public/03---resources/wsec-2017-fs-001-RDI/I-modeling-fact-sheet---final.pdf).

RDI/I causes sanitary sewers to experience increased flows that they are not designed to handle, contributing to sanitary sewer overflows (SSOs), which releases disease causing pathogens into the environment among other environmental concerns (Lai, 2008). The release of these pathogens influences the public agenda in multiple ways. In a report for the EPA, Fu-hsiung Lai states that

> SSO effects are many, including: (1) closing of beach and recreational areas; (2) prevention of fishing and shellfish harvesting; (3) public health risks associated with raw sewage in roadways, drainage ditches, basements, and surface waters; (4) inhibition of potential development from sewer connection moratoriums; and (5) financial liability of a community from public relation problems. In San Diego, CA, SSOs threatened drinking water supplies, creating the potential for serious adverse public health impact (Golden, 1996). (Lai, 2008, p. 2)

RDI/I also reduces the capacities of wastewater treatment plants (WWTPs). Stormwater that invades sanitary sewers as RDI/I comingles with sewage flows, forcing WWTPs to increase their loads while treating water that does not require treatment (Rödel et al., 2017).

Antecedent Moisture

RDI/I is influenced by the antecedent moisture condition of the environmental system it exists within. In his Master of Science in Civil Engineering Capstone project report, Dennis Weiland describes antecedent moisture as:

> How precipitation reacts depends on the water deficit. Was the system already dry or oversaturated? Is there surface water present to evaporate? Has ground water had time to settle, or is it above the normal levels? These conditions are summed together as antecedent moisture. Antecedent moisture is the preceding moisture condition of an environment. It is a complex representation of the relative wetness or dryness in the soil, also known as the soil moisture deficit. The wetness of the soil is impacted by many variables. Elevation, soil type, seasonal precipitation, impervious surfaces, temperature and more work together to define the state of the soil moisture deficit. At low

> temperatures, it is expected that there will be higher soil moisture content in the ground and less evapotranspiration and greater runoff will occur. (Weiland, 2020, p. 7)

The soil moisture deficit is an important factor of antecedent moisture and tends to change with the seasons. A lack of moisture deficit means the soil is more saturated, making it difficult for the soil to absorb water (Viessman et al., 1989). Colder seasons such as late fall, winter, and early spring have little to no soil moisture deficit, which results in rainwater not being absorbed by the soil. Instead, it infiltrates through the soil and joins the water table. Colder seasons tend to experience higher water table elevations due to the lack of moisture deficit impacting the antecedent moisture conditions. This results in higher volumes of RDI/I entering sewers through infiltration routes. During the warmer seasons of late spring and summer, the moisture deficit increases due to the increased evaporation and transpiration removing moisture from the soil. This results in stormwater being absorbed more readily as it infiltrates the soil, resulting in less water reaching the water table. Thus, RDI/I in warmer seasons primarily enters sewers through inflow routes.

Rain events themselves greatly impact antecedent moisture conditions and can compound to create intense RDI/I responses in sewer systems. For instance, if a rainfall event were to occur in the hot summer month of July when the soil moisture deficit is high, a higher percentage of precipitation would be absorbed by the soil and stored there due to its dry condition. However, if a rainfall event occurs in the day directly after the previous rainfall event, the precipitation will be falling during wet antecedent moisture conditions due to the ground remaining moist from the day prior. The moisture deficit is now lower, resulting in less moisture being absorbed by the soil and consequently higher volumes of infiltration are able to enter sewers. Compounding rainfall events also leads to higher quantities of RDI/I through inflow routes due to the soil’s ability to

absorb rainfall decreasing with each subsequent storm. Figure 3 displays an example of compounding rain events of similar magnitude leading to increasingly higher RDI/I volumes due to antecedent moisture conditions (Czachorski et al., 2022).

Figure 3

Increasing RDI/I Volumes due to Compounding Rainfall Events

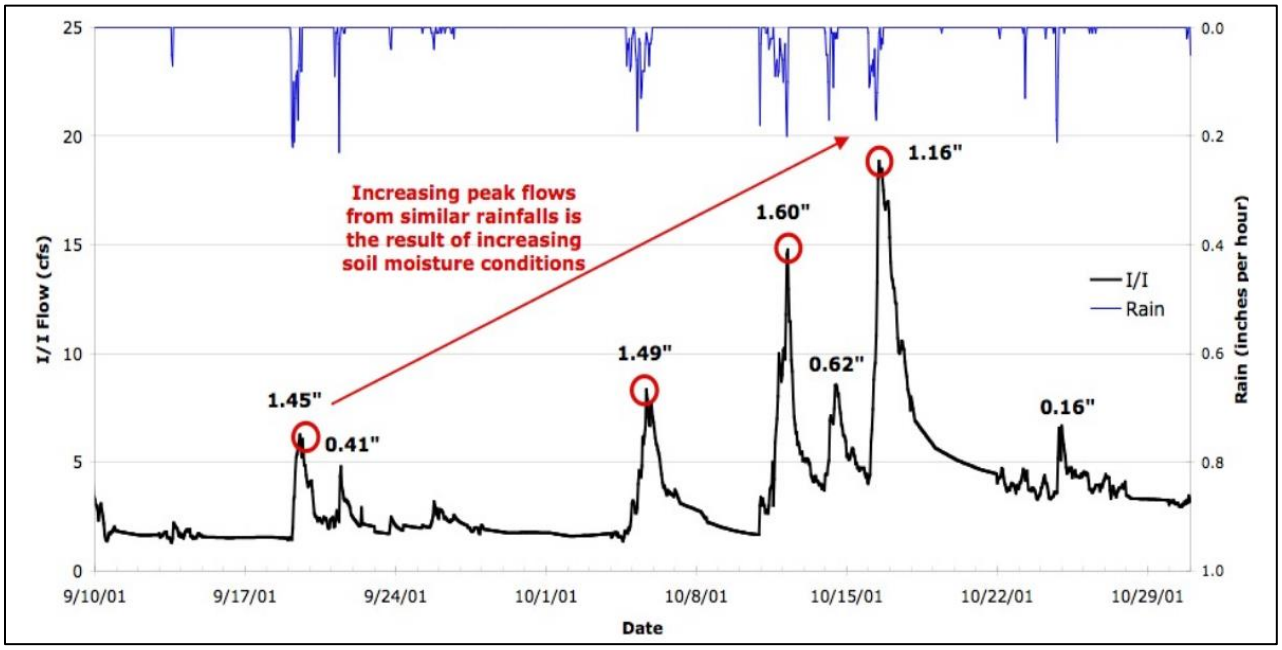

Note. Adapted from "AMM users conference", by R. Czachorski, D. Edgren, E. Morgan, & W. Gonwa, 2022, *H2Ometrics* (https://h2ometrics.com/amm-users-conference-2022/).

Sewer Flow Hydrographs and their Components

Hydrographs are the standard method for representing the flow of water over time in hydrology. They are graphs that display the flow or depth response in a sewer or waterway caused by hydrologic events such as rainfall and snowmelt over an area of land versus time, usually designated by a watershed. In *Introduction to Hydrology*, a watershed is defined as "the land area over which rain falls that contributes surface runoff to any point of interest" (Viessman

et al., 1989, p. 153). This study focuses entirely on sewer catchments, a type of watershed. A sewer catchment refers to the land area over which rain falls that contributes to a sewer's flow through RDI/I. Figure 4 displays an example of a sanitary sewer hydrograph, with its components denoted.

Figure 4

Example Sanitary Sewer Hydrograph

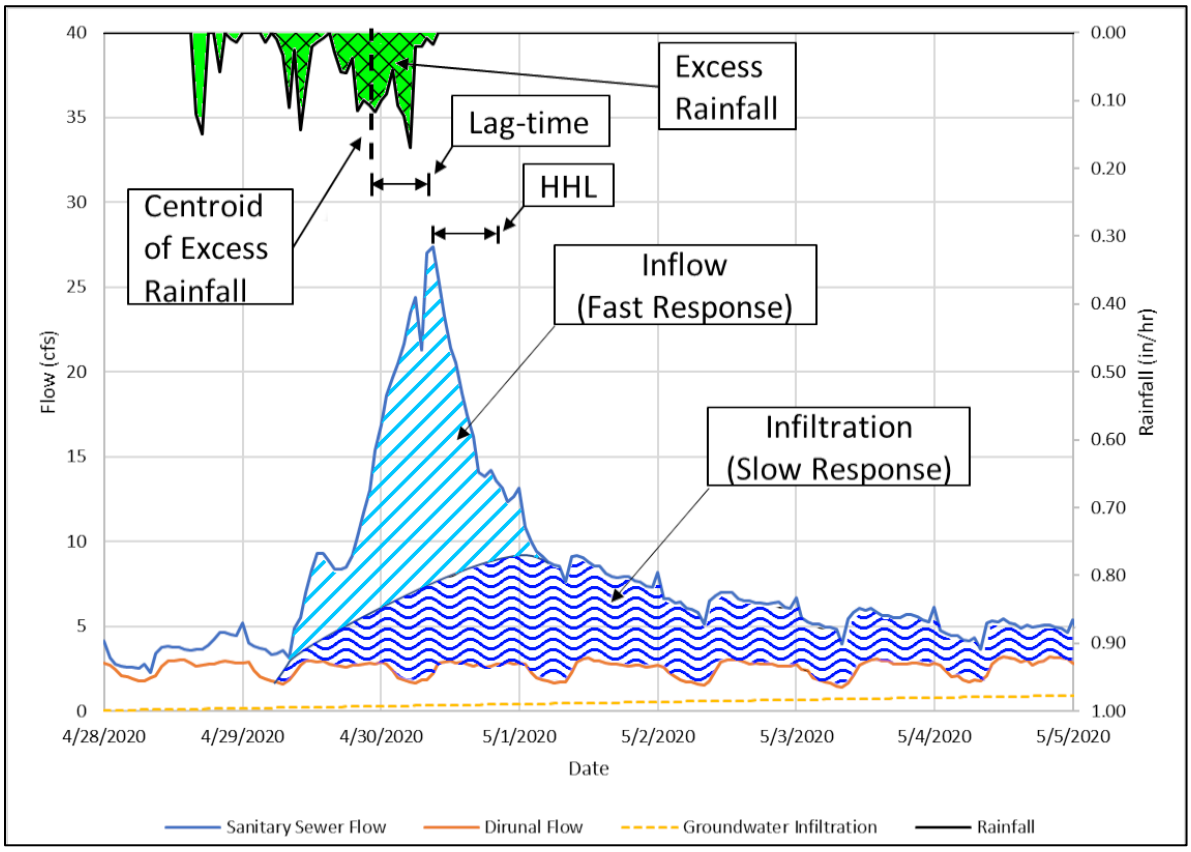

Note. Figure 4 displays a typical sanitary sewer hydrograph, created using data received from MMSD.

The hydrograph displayed in Figure 4 has many terms that relate to its overall structure, and they are defined below.

1. Rainfall: The line graph shaded green situated at the top left of Figure 4 represents the amount of rainfall that occurred during the hydrograph's timeframe. The rainfall is measured in units of inches per hour and provides an accurate estimate of the total volume of water introduced to the sewer's catchment area.
2. Excess Rainfall: The hatched area of the rainfall line graph represents the excess rainfall. Excess rainfall is the volume of rain that elicits a response in the sewer. In sanitary sewer systems, excess rainfall is a small fraction of total rainfall.
3. Inflow (Fast Response): The portion of the hydrograph that is comprised of the inflow component of RDI/I. Inflow represents water traveling along routes that are unimpeded or open, meaning it reaches the sewer much faster than infiltration routes. Therefore, the inflow is considered the fast response in the sewer system. It rises and falls quickly, forming the peak of RDI/I responses.
4. Infiltration (Slow Response): Infiltration represents water that isn't absorbed by the soil and makes its way into the sewer through infiltration routes. These flows slowly move through soil until they enter the sewer, and therefore, they are considered the slow response. Infiltration typically peaks in magnitude later than the inflow component as a result. Sewer catchment areas consisting mostly of rural land use and less impervious cover experience larger volumes of infiltration. The total volume of inflow and infiltration equals the volume of excess precipitation.
5. Lag-time: The elapsed time between the centroid of excess rainfall and the peak of sewer flow. The lag-time is an indicator of how quickly a sanitary sewer will experience peak flow conditions following a rainfall event. Sewers with catchment areas mostly consisting

of urban land use typically experience shorter lag-times due to an abundance of impervious surfaces leading to more water invading sewers through inflow routes.

6. Hydrograph half-life (HHL): The elapsed time between the peak flow value of a sewer's RDI/I response and a flow value of half the peak's magnitude. HHL is an indicator of a sewer catchment area's characteristics, with a shorter HHL indicating the sewer catchment is more uniform in shape or smaller in size than a catchment area with a higher HHL.
7. Diurnal flow: Represents the flows experienced by a sanitary sewer due to residential, commercial, and industrial wastewater or greywater. Diurnal flow, as evidenced by its name, varies on a daily basis. There is slight variation throughout the week as well, with weekends seeing higher peak flows than weekdays.
8. Groundwater infiltration: Groundwater fluctuations that occur over a long period of time, resulting in slightly increased sewer flow. Separate from the infiltration flow caused by RDI/I events.

Characteristics of a sewer's catchment area influence how quickly water reaches the sewer and the magnitude of the flow observed. The size of a catchment will influence the quantity of RDI/I observed, with larger catchments experiencing greater amounts of RDI/I due to water being captured over a greater area than smaller catchments (Cretu et al., 2005). The shape of a catchment area determines how quickly RDI/I can be conveyed to a sewer's metering point. Long, narrow catchment areas take longer to convey the RDI/I to a metering point due to the long distances the runoff must travel, resulting in higher times of concentration and lag (Cretu et al., 2005). Catchment areas that have more uniform shapes akin to circles have lower times of

concentration and lag because the average flow path is shorter that the runoff must travel along. (Cretu et al., 2005).

Components of Sanitary Sewer Flow

Sanitary sewer systems experience flows from a myriad of different sources. They can be split up into two different categories, dry weather flow (DWF) and wet weather flow (WWF). DWF includes components of sewer flow present during dry weather, absent of rainfall events. DWF is generally considered the normal flow state of a sanitary sewer system, uninfluenced by extraneous flow. WWF is experienced whenever extraneous water sources find their way into a sanitary sewer system, causing an RDI/I response in the sewer. WWF consists of the flows that make up RDI/I, inflow and infiltration. A diagram displaying the components of sanitary sewer flow can be seen in Figure 5.

Figure 5

Sanitary Sewer Flow Components

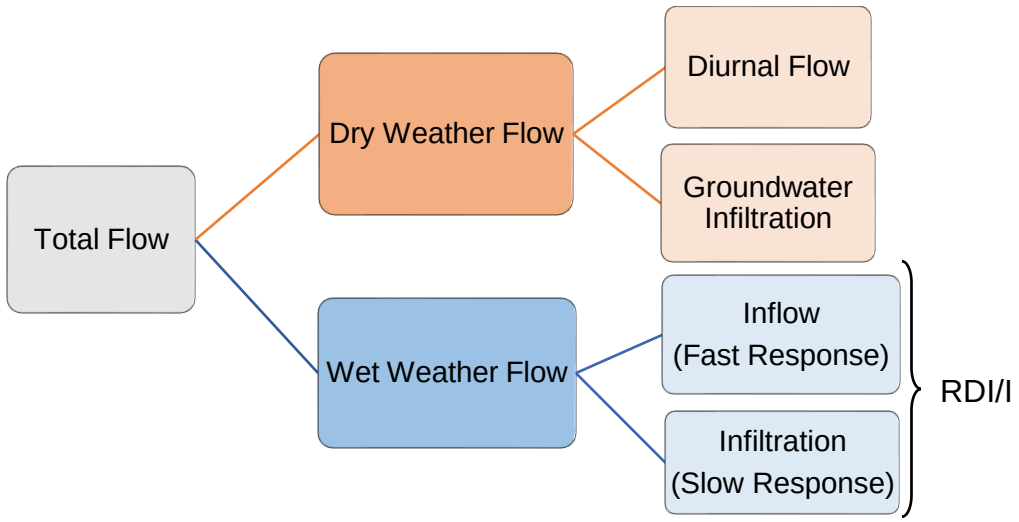

Sanitary Sewer Dry Weather Flow Component

DWF includes diurnal flow and groundwater infiltration (GWI). DWF is explained well by Fu-hsiung Lai in a report developed for the EPA:

> The [DWF] component primarily includes sanitary flow contribution from residential, commercial, industrial, and institutional users. [DWF] rates typically vary throughout the day, with the peak flow generally occurring during the morning hours. It also includes some amount of groundwater infiltration (GWI), particularly in areas where groundwater table is high. (Lai, 2008, p. 6)

The portion of GWI that occurs during dry weather is a result of long-term fluctuations in groundwater elevations throughout the changing seasons. During spring months when wet antecedent moisture conditions are more common, groundwater levels are elevated, resulting in more of it infiltrating into sewers (Lai, 2008). The magnitude of GWI experienced by a sanitary sewer system is proportional to the number of defects present in the sewer and their sizes (Lai, 2008).

Sanitary sewer system design typically calculates diurnal flow based on a per capita flowrate estimate for each resident the system is servicing (Zanoni & Rutkowski, 1972). It is the first component of flow considered in the sizing of a sanitary sewer since it’s relatively predictable due to swathes of historical data existing for sewage flow by capita (Zanoni & Rutkowski, 1972). However, sanitary sewer system design must account for extraneous flows experienced during WWF as well.

Sanitary Sewer Wet Weather Flow Component

Whenever a rainfall event occurs near a sanitary sewer system, WWF begins during or shortly after. The delay in the start of WWF conditions depends on the characteristics of the watershed the sewer is a part of. Sanitary sewer systems that have catchment areas with longer lag-times will experience WWF later than sewers with catchment areas possessing shorter lag-times. A hydrograph displaying the typical flow components of a sanitary sewer system, including WWF, was pictured in the sewer flow hydrographs and their components section in Figure 4.

WWF consists of additional extraneous flows that invade sewers during or after rainfall and snowmelt. These extraneous flows are RDI/I, whose components influence the sewer's hydrograph at differing speeds. Inflow sources of RDI/I are the first to contribute to the sanitary sewer's flow as they enter through open pathways with little to no resistance (WEF Collection Systems Committee, 2017). This is exemplified in Figure 4 by the large spike in sewer flow after the majority of rainfall has occurred. After RDI/I's inflow component has entered the sewer system, the infiltration component slowly enters through cracks, faulty connections, and root intrusions (WEF Collection Systems Committee, 2017). Infiltration is slowly added to the sanitary sewer's flow and results in a gradual decay in sewer flow as its volume is depleted. RDI/I plays a large role in sanitary sewer flow during WWF and must be accounted for during the sewer design process to limit SSOs and increased WWTP loads (Sola et al., 2020). Modeling the RDI/I components of WWF utilizing AMM will be the main focus of this paper.

Antecedent Moisture Modeling

Antecedent moisture modeling is a procedure created by Robert Czachorski and Tobin Van Pelt that estimates a time series of a sanitary sewer's RDI/I flow at a specified outlet based

on a moving average precipitation and ambient air temperature over the watershed (Van Pelt & Czachorski, 2002). AMM's first iteration was introduced to the public domain in 2021; however, it has since been updated and reparametrized (Edgren et al., 2023). In a manuscript submitted for publication, Edgren et al. (2023) describe the four types of enhancements to AMM's first iteration:

1. Improving physical relatability – Reparameterized the original model so that the parameters are intuitively understandable to users and the units are explicitly stated.
2. Creating scale independence – With the original equations, scaling a calibrated AMM model to a catchment of a different size requires scaling 3 different parameters. The new parameterization explicitly includes catchment area which allows direct comparisons in parameter values between differently-sized catchments.
3. Creating timestep independence – With the original equations, some parameters were timestep dependent, requiring conversion to different timestep. The new equations have parameters that are independent of timestep.
4. Updating nomenclature – Some minor improvements were made to make the nomenclature simpler and more intuitive. (Edgren et al., 2023, p. 3)

The focus of this paper will therefore lie entirely on the new parameterization of AMM as it is the most current form of the AMM procedure.

AMM consists of three levels, with each level containing its own set of equations. Each level's output feeds into the subsequent level, with Level 3 feeding into Level 2, and Level 2 feeding into Level 1. Level 1 contains the final set of equations computed and outputs the predicted flow series. The equations given by Edgren et al. (2023) are

$$Q_t = A * \left(RD + \frac{RW_t + RW_{t-1}}{2}\right) * MAP_t * \frac{(1-SF)}{\Delta t} + SF * Q_{t-1}, \quad (1)$$

$$SF = 0.5^{(\Delta t/HHL)}, \quad (2)$$

$$MAP_t = \frac{1}{\frac{PAT}{\Delta t} + 1} \sum_{i=1}^{\frac{PAT}{\Delta t}+1} P_{t-i}, \quad (3)$$

where

Q_t = Flow rate at the current time step *t* [L^3/T],

A = Catchment area [L^2],

RD = minimum rainfall capture fraction during dry weather [%],

RW_t = Additional rainfall capture fraction during wet weather [%],

SF = Constant shape factor of hydrograph, bounded by [0,1],

Δt = Model time step [T],

Q_{t-1} = Flow rate at the previous time step *t–1* [L^3/T],

MAP_t = Moving average incremental precipitation at time step *t*, [L],

PAT = Precipitation averaging time of the catchment (integer multiple of Δt) [T],

P_{t-i} = Incremental precipitation starting at time step *t–i*, where *i* varies from 1 to *PAT/Δt+1* [L],

HHL = Hydrograph half-life [T].

The parameter RW_t changes over time, allowing the wet weather capture fraction to adjust to the catchment area's changing moisture conditions. Therefore, RW_t is a time series and is determined by the Level 2 equations of AMM.

Level 2 of AMM is calculated as an intermediate step between Levels 1 and 3 and determines the impact of antecedent moisture on the RW_t time series. Level 2's equation set produces the RW_t time series and the equations given by Edgren et al. (2023) are

$$RW_t = \frac{(AMRF-1)}{ln(AMRF)} * SHCF_t * MAP_t + AMRF * RW_{t-1} , \quad (4)$$

$$AMRF = 0.5^{(\Delta t/AMHL)}, \quad (5)$$

where

RW_{t-1} = Additional wet weather rainfall capture fraction at the previous time step *t-1* [%],

$SHCF_t$ = Seasonal hydrologic condition factor at current time step t [1/L],

AMRF = Constant antecedent moisture retention factor, bound by [0,1],

AMHL = antecedent moisture half-life [T].

The AMHL is a calibratable parameter that determines how quickly the system dries, effectively representing the duration of antecedent moisture effects on the system (Edgren et al., 2023). The $SHCF_t$ changes with respect to the moving average temperature series ($MATemp_t$) of the catchment area and is calculated in Level 3 of AMM.

Level 3 of AMM is the first set of equations to be calculated and produces the seasonal hydrologic condition factor time series ($SCHF_t$). The $SHCF_t$ is the driving time series for the

RW_t time series and determines how quickly the RW_t time series increases due to rainfall. The equations given by Edgren et al. (2023) are

$$SHCF_t = \left[\frac{L}{1 + e^{(-k\{MATemp_t - x_o\})}}\right] + Cold\ SHCF - \frac{11}{12}L, \tag{6}$$

$$L = 1.2 \times (Cold\ SHCF - Hot\ SHCF), \tag{7}$$

$$k = \left[\frac{4.7964}{(Cold\ Temp - Hot\ Temp)}\right], \tag{8}$$

$$x_0 = \frac{(Cold\ Temp + Hot\ Temp)}{2}, \tag{9}$$

$$MATemp_t = \frac{1}{\frac{TAT}{\Delta t} + 1} \sum_{i=1}^{\frac{TAT}{\Delta t} + 1} Temp_{t-i}, \tag{10}$$

where

Cold SHCF = Cold seasonal hydrologic condition factor value from Point 1 [1/L],

Hot SHCF = Hot seasonal hydrologic condition factor value from Point 2 [1/L],

Cold Temp = Cold temperature value from Point 1 [Temp],

Hot Temp = Hot temperature value from Point 2 [Temp],

$MATemp_t$ = Moving average temperature at time step *t* [Temp],

TAT = Temperature averaging time of the catchment (increments of Δt) [T],

$Temp_{t-i}$ = Air temperature at time step t-i, where i varies from 0 to $TAT/\Delta t$ [Temp],

L = Range of variation of the seasonal hydrologic condition factor [1/L],

x_0 = Midpoint between the hot and cold temperature values [Temp],

k = Factor indicating the sigmoid function steepness [1/Temp],

Point 1 = location in sigmoid function that represents 11/12 of maximum range of seasonal hydrologic condition factor (see Figure 6),

Point 2 = location in sigmoid function that represents 1/12 of maximum range of seasonal hydrologic condition factor (see Figure 6).

Figure 6

Sigmoid Function Representing the Variation of the SHCF in AMM

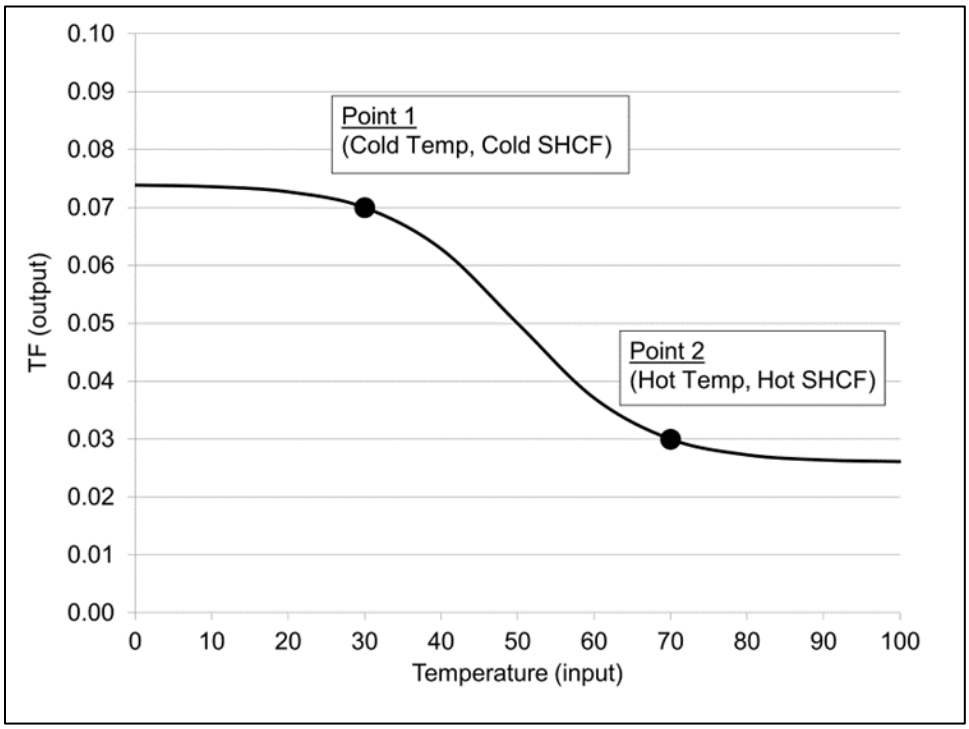

Note. Adapted from "AMM Users Conference", by R. Czachorski, D. Edgren, E. Morgan, and W. Gonwa, 2022, *H2Ometrics*. Retrieved from https://h2ometrics.com/amm-users-conference-2022/. The graph shows a sigmoid curve, which represents the SHCF that corresponds to the timestep's temperature. Point 1 and 2 on the curve are determined by parameters input by the user, the cold and hot SHCF. As temperature increases, the SHCF decreases.

When the SHCF increases due to colder temperatures, the RW_t time series increases rapidly in response to additional rainfall (Edgren et al., 2023). Conversely, when the SHCF decreases due to hotter temperatures the RW_t time series requires more rainfall to increase by a similar amount (Edgren et al., 2023).

A diagram explaining how each level feeds into the next in AMM is displayed in Figure 7.

Figure 7

AMM Overview Schematic

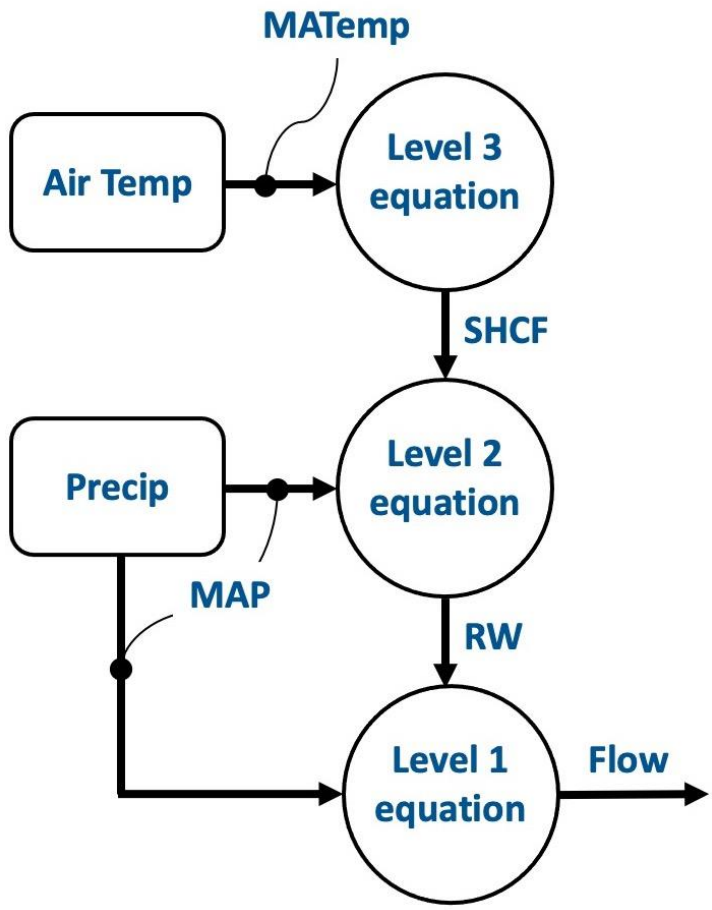

Note. Adapted from D. Edgren, R. Czachorski, and W. Gonwa, 2023, *Reparameterizing the antecedent moisture model* [Manuscript submitted for publication].

Utilizing AMM to accurately predict RDI/I flows to sanitary sewers typically involves the use of two different flow types, which are then summed to represent the total WWF hydrograph. Usually designated as fast and slow response, they represent the inflow and infiltration components of RDI/I, respectively. Each flow is calculated using the three levels of AMM, and each have their own set of parameters listed in the equations above. However, many parameters

are either fixed or calculated during calibration such as the catchment area, A, in Equation (1) or the range, L, in Equation (7). Edgren et al. (2023, p. 9) state that there are six parameters typically calibrated during AMM, including:

1. RD – Rainfall Capture Fraction during very dry conditions
2. PAT – Precipitation averaging time
3. HHL – Hydrograph recession time
4. AMHL – Drying time; duration of antecedent moisture effect
5. Cold SHCF – Unit increase in Rainfall Capture Fraction in winter
6. Hot SHCF – Unit decrease in Rainfall Capture Fraction in summer.

Calibration of the aforementioned parameters was the main method of producing comparable results between temperature-based AMM and AMM using streamflow signals.

Implementation of a Streamflow Signal in Antecedent Moisture Modeling

The implementation of a streamflow signal in AMM was achieved through two methods. The first method implemented was the two-level method, which scales a streamflow time series to a value between 0 to 1, with 0 being the minimum of the time series and 1 being the maximum. The second method implemented was the three-level method, which scales a streamflow time series to a value between 30 to 70 to represent the temperature time series in the third level of AMM. The 30 value represents the maximum value of the streamflow time series while 70 represents the minimum, following the standards of temperature-based AMM, which sees a higher SHCF when temperatures are lower.

Two-Level Streamflow Method

The reason this method is called the two-level method is due to the fact that it utilizes only the first two levels of AMM. The two-level method's scaled streamflow value, which ranges between 0 to 1, eliminates the need for the SHCF time series created by the third level of AMM. The two-level method's equations are

$$RW_t = RW_{max} * Scaled\,MASF_t^2, \tag{11}$$

$$Scaled\,MASF_t^2 = \frac{MASF_t - MASF_{min}}{MASF_{max} - MASF_{min}}, \tag{12}$$

$$MASF_t = \frac{1}{\frac{SAT}{\Delta t} + 1} \sum_{i=1}^{\frac{SAT}{\Delta t}+1} SF_{t-i} \quad , \tag{13}$$

where

RW_{max} = Maximum wet weather capture fraction designated by user [%],

Scaled $MASF^2_t$ = Moving average of streamflow time series at timestep *t*, scaled to a value between 0 and 1 (the exponent 2 designates this as the two-level scaled $MASF_t$ parameter) [%],

$MASF_t$ = Moving average of streamflow time series at timestep *t* [L^3/T],

$MASF_{min}$ = Minimum of $MASF_t$ [L^3/T],

$MASF_{max}$ = Maximum of $MASF_t$ [L^3/T],

SFAT = Streamflow averaging time of the catchment (increments of Δt) [T],

SF_{t-i} = Streamflow at time step *t-i*, where *i* varies from 0 to $SFAT/\Delta t$ [L^3/T].

In this method, Equation (11) replaces Equation (4) in temperature-based AMM, and the scaled $MASF^2_t$ time series represents the SHCF time series utilized in temperature-based AMM. Equation (1) is retained as the first level output equation in this method. The two-level method assumes that as the catchment area's antecedent moisture conditions grow wetter, the $MASF_t$ parameter increases. Therefore, a scaled $MASF_t$ value of 0 represents the minimum flow value of the $MASF_t$ time series while a value of 1 represents the maximum flow value.

The two-level method removes the need for a third level equation set, thus reducing the number of calibratable parameters from six to four. The four calibratable parameters of the two-level method include:

1. RD – Rainfall capture fraction during very dry conditions
2. RDW_{max} – Maximum rainfall capture fraction during wet conditions
3. HHL – Hydrograph recession time
4. PAT – Precipitation averaging time.

Three-Level Streamflow Method

Like the two-level method, the three-level method's name stems from the fact that it utilizes all three levels of temperature-based AMM. In the three-level method, the moving average streamflow time series, $MASF_t$, is scaled to a range of 30 to 70 and replaces the moving average temperature time series input, $MATemp_t$, in Equation (6) of temperature-based AMM. The three-level method's equations are

$$SHCF_t = \left[\frac{L}{1 + e^{(-k\{Scaled\ MASF^3_t - x_o\})}}\right] + Cold\ SHCF - \frac{11}{12}L \quad (14)$$

and

$$Scaled\ MASF_t^3 = 70 - \left[\frac{MASF_t - MASF_{min}}{MASF_{max} - MASF_{min}} * 40\right]. \quad (15)$$

The three-level follows the same assumption as the two-level method, in that the catchment area's antecedent moisture conditions grow wetter as the $MASF_t$ increases. It follows the same standards as temperature-based AMM. As the $MASF_t$ increases, the scaled $MASF^3_t$ emulates the temperature signal by decreasing in magnitude. Therefore, as the streamflow signal increases in magnitude, the $SHCF_t$ increases as well, correlating increasing streamflow to increasingly wet antecedent moisture condition.

The three-level method utilizes the same number of calibratable parameters as temperature-based AMM. The only difference lies in the replacement of temperature-based AMM's temperature averaging time parameter, TAT, with the three-level method's streamflow averaging time parameter, SFAT. However, TAT is typically fixed early on in the AMM calibration process; thus, SFAT isn't a calibratable parameter. Therefore, the six calibratable parameters of the three-level method include:

1. RD – Rainfall Capture Fraction during very dry conditions
2. PAT – Precipitation averaging time
3. HHL – Hydrograph recession time
4. AMHL – Drying time; duration of antecedent moisture effect
5. Cold SHCF – Unit increase in Rainfall Capture Fraction in winter
6. Hot SHCF – Unit decrease in Rainfall Capture Fraction in summer.

Bayesian Optimization

Bayesian optimization is an algorithm that can be employed in a variety of different coding languages. MATLAB was the coding language chosen to implement the Bayesian

optimization algorithm to assist in the calibration of various AMM parameters. The algorithm is based on Bayes' theorem, which was conceived by the British mathematician Thomas Bayes in 1763 (Hayes, 2022). Bayes' theorem's core principle lies in determining conditional probability, which is the likelihood of an outcome occurring based on a previous outcome having occurred in similar circumstances (Hayes, 2022). According to Hayes (2022), "Bayes' Theorem states that the conditional probability of an event, based on the occurrence of another event, is equal to the likelihood of the second event given the first event multiplied by the probability of the first event" (para. 18).

Essentially, the Bayesian optimization algorithm allows for automated calibration of AMM parameters. The user specifies the main function for the algorithm to input its parameters, as well as specifying a range for the given parameters. The algorithm then guesses a random value for each parameter in the given ranges, and uses a loss function that, in this case, displays the average error value of the observed flow versus the predicted flow. It is an iterative process, and initially the error increases while the algorithm inputs random values of the user-specified range. However, an increasing error value allows the algorithm to determine that the values it is attempting are straying further from its goal, the lowest achievable error value utilizing the parameters and their given ranges. The algorithm can then start to either lower or raise certain values of the parameters based on the outcomes of its previous guesses, assembling a probability of what its most optimal next guess is.

For instance, the Bayesian optimization algorithm may initially guess that a catchment area has a RD value of 0.5. The error value increases, and subsequently a guess of 0.6 is made. The error value increases again, allowing the algorithm to understand that increasing the RD parameters correlates with an increase in error. Therefore, its next guess is 0.45, which lowers

the error value. This process repeats until the algorithm has performed a set number of iterations defined by the user. This process is useful for determining AMM parameters when fast and slow flow types are utilized, which doubles the number of calibratable parameters. Bayesian Optimization greatly assists in the calibration of parameters that are more difficult to calibrate such as the Cold / Hot SCHF, PAT, and RW_{max}.

Study Area Properties and Metering Locations

The Milwaukee area was designated as the study area of this paper due to the abundance of available data for the area's sanitary sewer flows, streamflows, and rain gages. Two sanitary sewers were selected for analysis, sewers MS0453 and MS0456. The two sewers were chosen due to their stark difference in average flowrates. MS0453 experienced average hourly flowrates of 2.56 cubic feet per second (cfs) throughout 2018 while MS0456 experienced only 0.32 cfs. Similarly, the catchment areas for each of the sewers were representative of their average flows, with MS0453 and MS0456 having catchment areas of 11,305 and 340 acres, respectively. The sewer's catchment areas also differ in land use, with MS0453's catchment area containing a mixture of rural and urban residential while MS0456's catchment area is entirely urban residential. Two rain gages, WS1214 and WS1224, were selected due to their proximity to the sewer's catchment areas. The rain gages and sewer metering locations as well as the sewer's catchment areas are depicted in Figure 8.

Figure 8

Locations of Sewer Meters, Sewer Catchment Areas, and Rain Gages Employed in Study

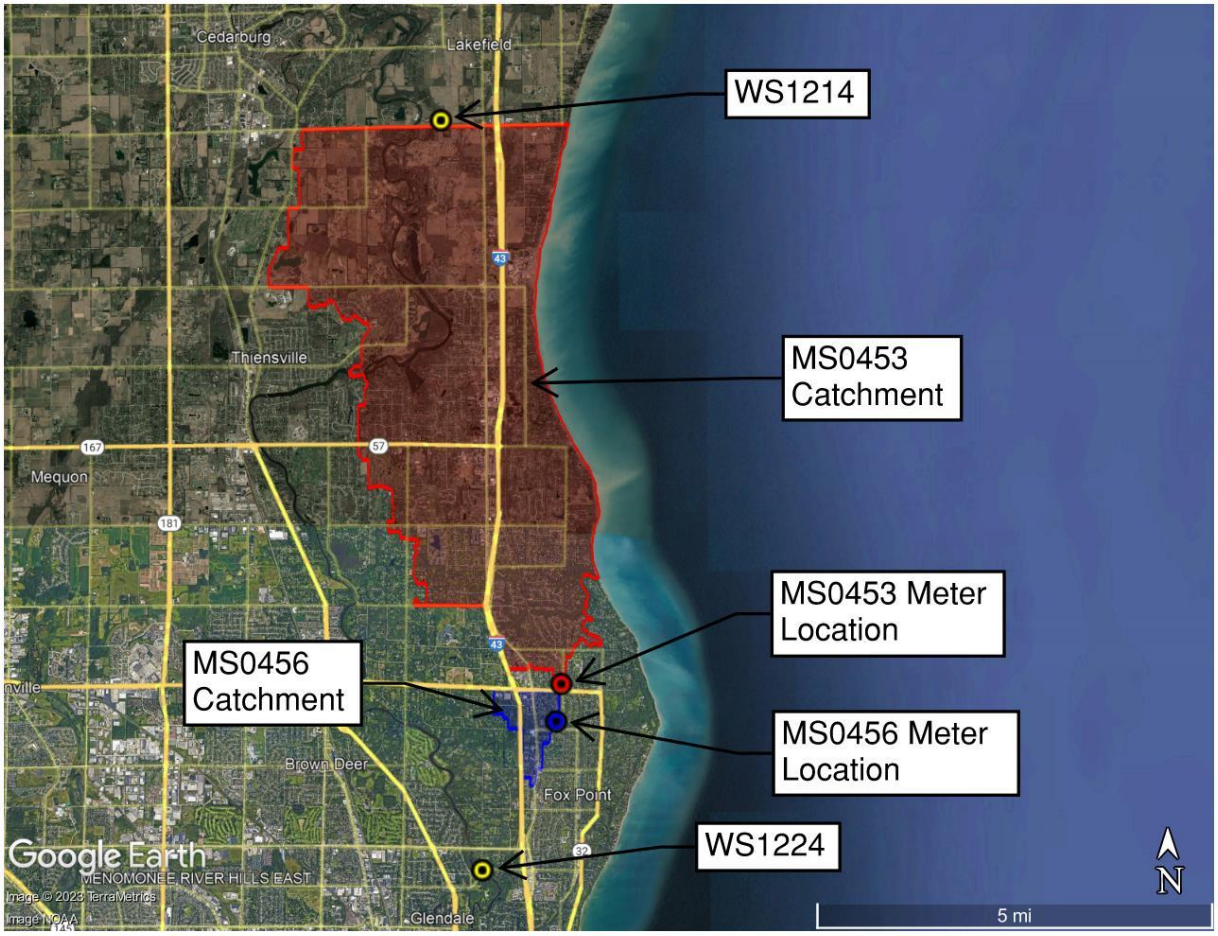

Note. Created using Google Earth Pro and MMSD provided sewer catchment area data.

After the selection of sewers MS0453 and MS0456, representative streamflows were selected to be implemented in AMM. Two streams were selected: Lincoln Creek and the Milwaukee River. The main reason for this selection lies in the fact that the two streams are the closest streamflows to the metering locations of sewers MS0453 and MS0456. The two streams are diverse in their flow magnitudes, similar to sewers MS0453 and MS0456, with Lincoln

Creek experiencing an average flow of 21.1 cfs during 2018 while the Milwaukee River experienced an average flow of 864.9 during the same time period. Figure 9 depicts the metering locations and watersheds of the two streams.

Figure 9

Locations of Streamflow Meters and Watersheds Employed in Study

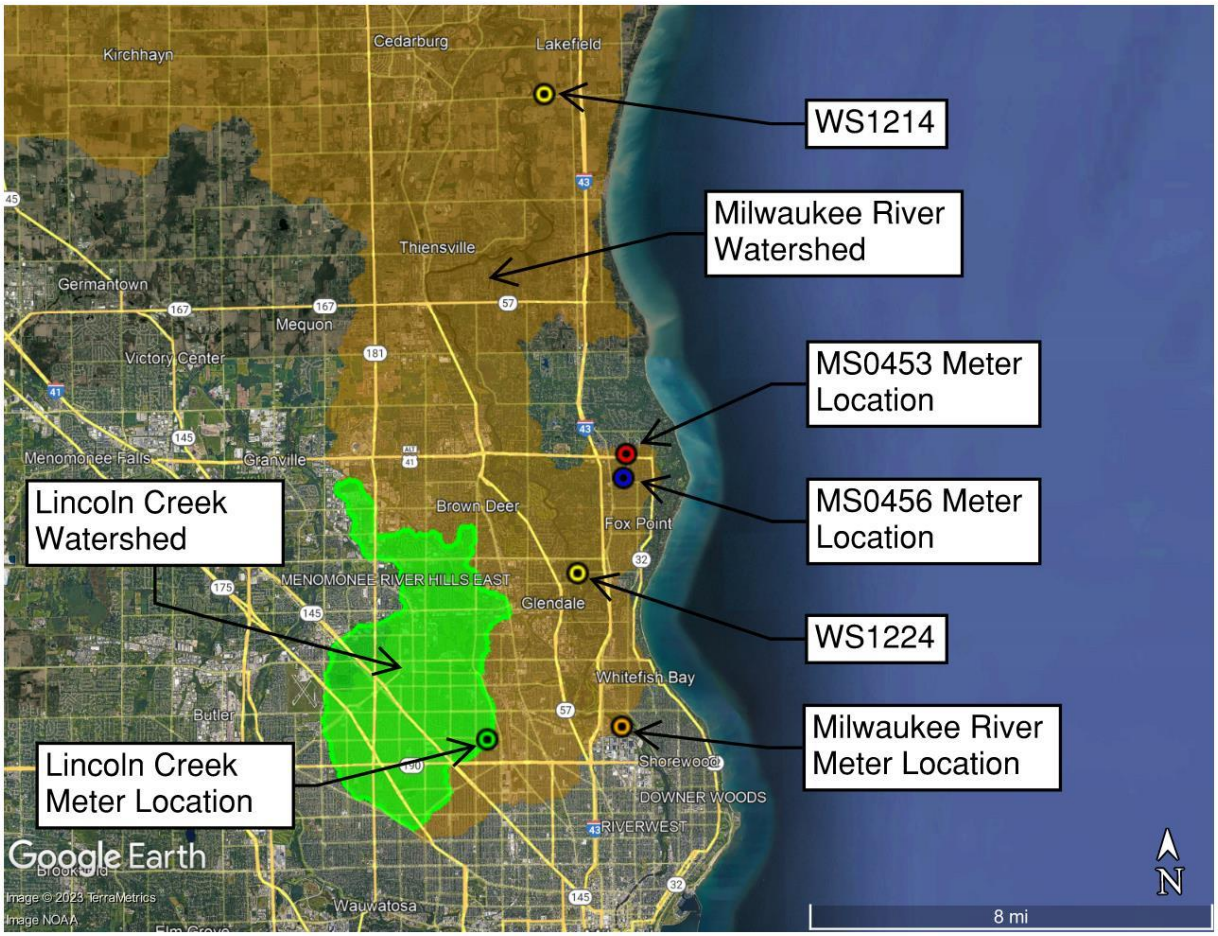

Note. Created using Google Earth Pro, streamflow gage locations and watersheds obtained through the USGS StreamStats tool. Retrieved from https://streamstats.usgs.gov/ss/

Methodology

The time range of this study was from January 1, 2018 to October 11, 2022, a time period of nearly five years. The data sources utilized were required to have complete records during the entire time period of the study; thus, each data set listed hereinafter has complete records during the specified time period.

Sanitary sewer flow data for sewers MS0453 and MS0456 were obtained from the Milwaukee Metropolitan Sewage District (MMSD). The sewer flow data received was reported in one-hour timesteps, the designated timestep for all AMM performed in this study. H2Ometrics was employed to isolate the WWF of the sewer flow data. H2Ometrics, a cloud-based water and sewer data program created by Robert Czachorski, contains a diurnal flow analysis tool which isolates the diurnal flow of a given sewer system (Czachorski, H2Ometrics, 2010). The diurnal flow produced using this analysis tool also accounts for long term variation due to GWI present during DWF. The diurnal flow (including GWI) was then subtracted from each sewer flow, leaving only the WWF due to RDI/I.

Streamflow data were gathered from USGS gages for the specified time period, specifically stations 04087000 and 040869416 of the Milwaukee River and Lincoln Creek, respectively (USGS, n.d.). Unlike the MMSD-provided sewer flow data, the timesteps of the data acquired from USGS's database varied over time. An interpolation function was utilized in Excel to approximate the flow values at the beginning of each hour, converting the data to a one-hour timestep.

Rain gage data were obtained from MMSD for the selected rain gages, WS1214 and WS1224, in one-hour timesteps. They were initially received in a cumulative format, meaning that each rainfall event added on to the previous depth recorded during a single day. At the end

of the day, the rainfall depth was reset to zero inches. The data were converted to an incremental format using Excel, meaning the precipitation depth recorded during a single hour was limited to that timestep. This allowed for the data to be utilized in AMM, which requires an incremental precipitation signal. WS1244 was designated as the representative rainfall signal for predicting sewer MS0456's flow using AMM due to the station being the closest in proximity to its catchment area as seen in Figure 8. Because sewer MS0453's catchment area is positioned between WS1224 and WS1214, the Theissen Polygon method was used to determine how much of its catchment area should be associated with each rain gage. Of sewer MS0453's 11,305 acre catchment area, 2,822 acres (25% of the total acreage) were found to be closer to WS1224 and 8,483 acres (75% of the total acreage) were found to be closer to WS1214. Therefore, a composite rainfall signal was created for AMM applications regarding sewer MS0453, consisting of a weighted average between WS1224 and WS1214 (WS1224 and WS1214 were assigned weights of 25% and 75%, respectively).

Temperature data were acquired through the National Oceanic and Atmospheric Administration's (NOAA) National Centers for Environmental Information (NCEI) Climate Data Online portal for the specified time period (NCEI, n.d.). The closest station with complete records for the time period of this study was Milwaukee Mitchell International Airport. However, the smallest timestep available for a temperature data request using the portal was 24 hours (average daily temperature). Therefore, the data were interpolated using a function in Excel to convert the data from a 24-hour timestep to a one-hour timestep.

Snow depth data were acquired through the NOAA's NCEI Climate Data Online portal for the specified time period (NCEI, n.d.). The closest station with complete records for the time period of this study was Milwaukee Mitchell International Airport. The smallest available

timestep for the snow depth data was 24 hours (average daily depth). However, the snow data did not require interpolation to a one-hour timestep as they are not an input in AMM. Snow depth was used to scrub the RDI/I responses to snowmelt events present in the sewer flow data, which is described in the following section.

Scrubbing the Data

After the required data were gathered, they were then scrubbed to ensure continuity, to remove erroneous sewer meter readings, and to remove snowmelt event influenced RDI/I responses.

When analyzing the stream and sewer flow data sets acquired for this study, there were several instances where the metering devices reported a flow of zero cfs. These instances could have occurred from many different factors, but the most likely cause is that the metering device errored when it recorded that specific flow value. In order to ensure continuity, each instance of a flow meter reporting a flow of zero cfs was examined. If flow values were observed before and after the zero cfs reading, the zero cfs value was replaced with an average of the previous and following flow value.

There were several instances where rainfall occurred over the sewers' catchment areas and there was no RDI/I response recorded by the sewer. Typically, the inflow component of RDI/I is nearly instantaneous, regardless of antecedent moisture conditions, as runoff enters sewers rapidly through connected roof drains and leaky manhole covers. A complete lack of RDI/I response in a sanitary sewer is unlikely due to these various inflow routes. Ultimately, there is no way to determine the exact cause of these occurrences and there is no ability to account for them using AMM due to AMM relying on RD, a constant capture fraction (W. Gonwa, personal communication, February 3, 2023). These erroneous sewer meter reading

events were therefore excluded in error calculations for all applications of AMM in this study. An example of a sewer meter discrepancy is depicted in Figure 10.

Figure 10

Erroneous Sewer Meter Reading Event

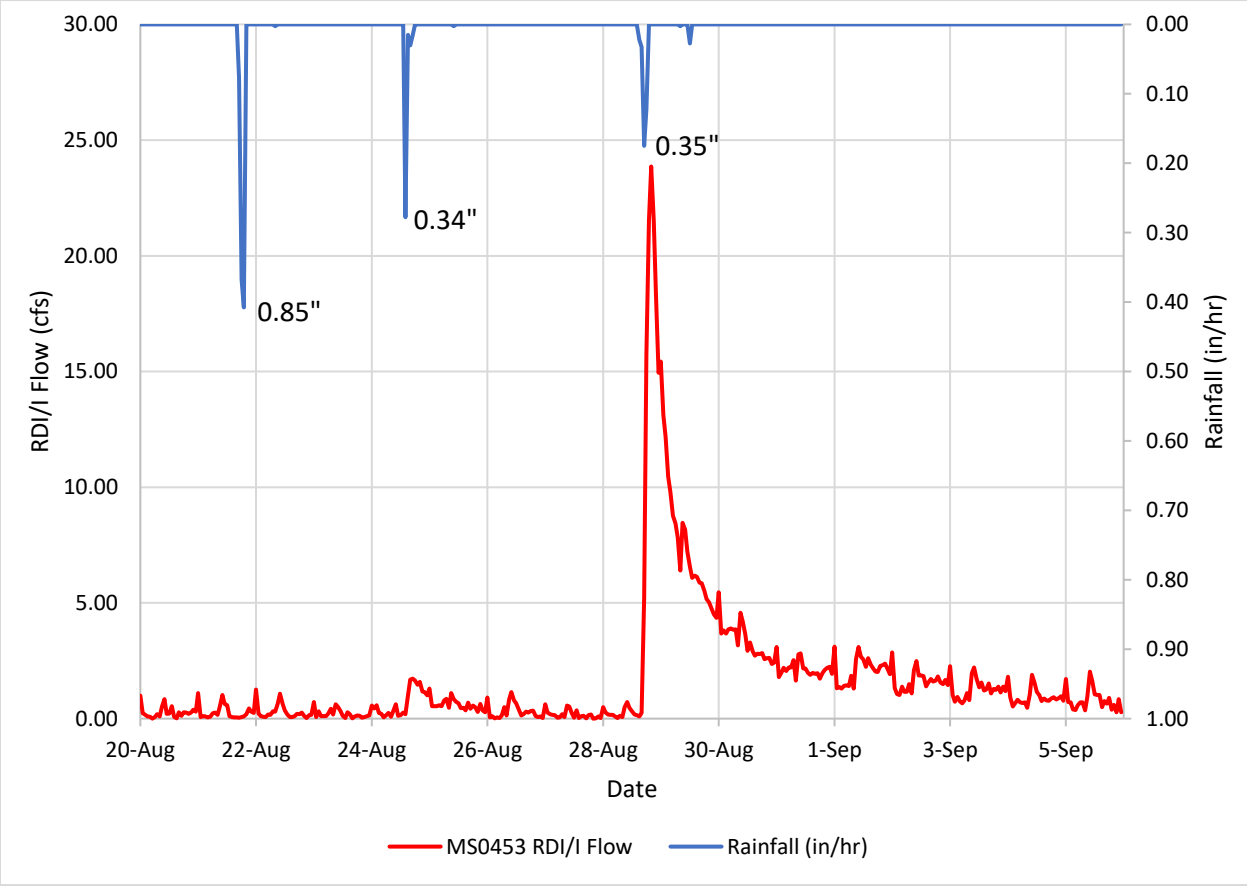

Note. Figure 10 shows the RDI/I flow experienced by sewer MS0453 as well as three rainfall events that occurred over its catchment area. The cumulative rainfall depths for each event are listed next to each event's peak rainfall intensity. Though the first event has a cumulative depth more than twice the depth of the third event, the third event was the only event to exhibit an RDI/I response in sewer MS0453.

AMM cannot account for RDI/I responses due to snowmelt. Snowmelt is not implemented in AMM in its current form. Using representative snow depth data, the RDI/I

responses due to snowmelt events were identified and removed from error calculations in order to reduce error associated with scenarios AMM was not designed for. Figure 11 shows an RDI/I response caused by a snowmelt event.

Figure 11

RDI/I Response due to Snowmelt Event

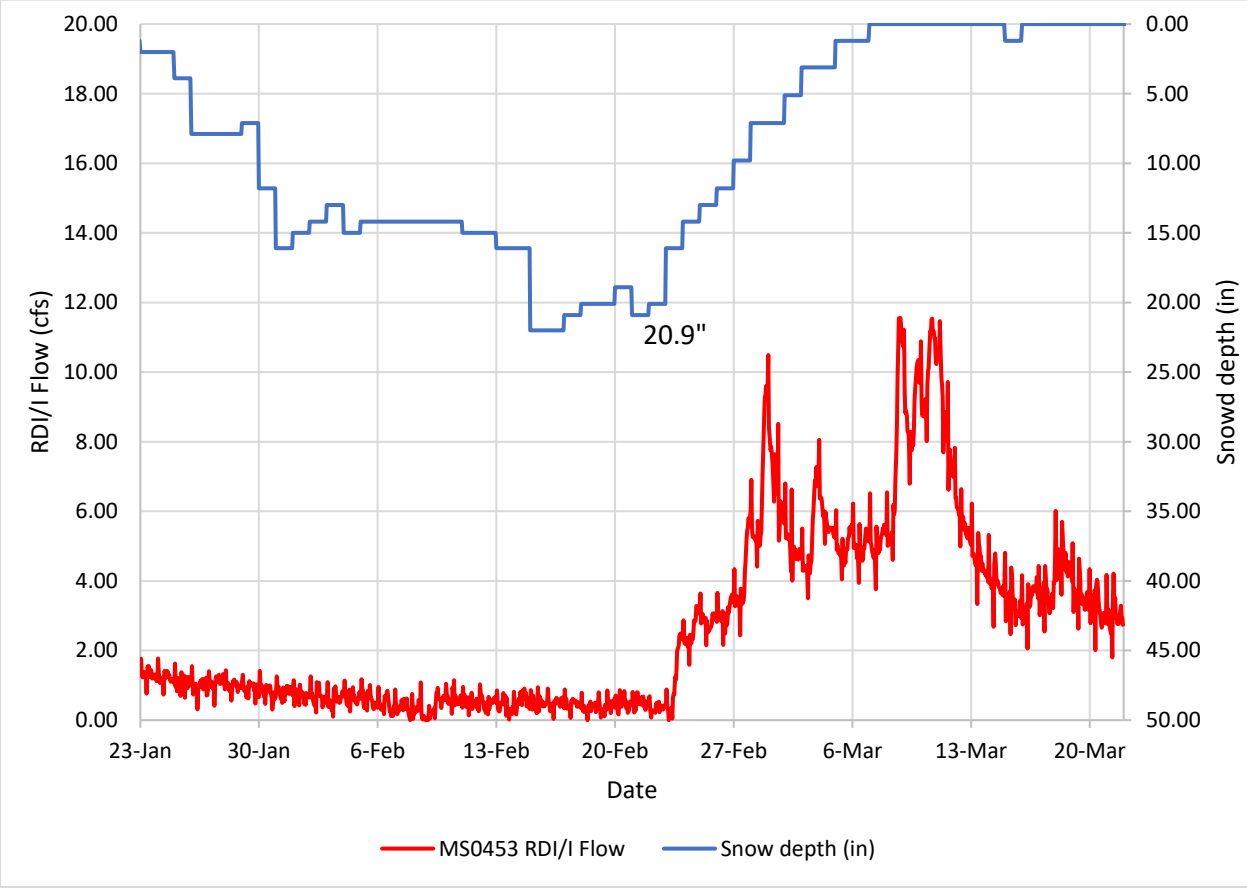

Note. Figure 11 shows the RDI/I response of sewer MS0453 due to a snowmelt event beginning around February 20, 2021. As the snow depth decreased from its peak of 20.9 inches, an increase in MS0453's flow was observed.

Sewer Hydrology Models

After scrubbing the data, they were imported to Excel. Eight different models were created, four for each sanitary sewer. They are listed as follows:

1. Sewer MS0453
    a. Temperature-based AMM model
    b. Milwaukee River two-level streamflow model
    c. Milwaukee River three-level streamflow model
    d. Lincoln Creek three-level streamflow model
2. Sewer MS0456
    a. Temperature-based AMM model
    b. Milwaukee River two-level streamflow model
    c. Lincoln Creek two-level streamflow model
    d. Lincoln Creek three-level streamflow model

Each of the models listed above utilized a fast and slow response, each with its own set of equations and calibratable parameters. The fast response represents the inflow component of the RDI/I response, while the slow response represents the infiltration component. The sum of the two responses represents the final predicted flow value. The variables calibrated for the temperature-based AMM models included RD, HHL, AMHL, PAT, Hot SHCF, and Cold SHCF. For the three-level streamflow models, the calibratable parameters were identical. For the two-level streamflow models, the calibratable parameters included RD, RW_{max}, HHL, and PAT. Many values had to be calibrated differently depending on if they represented the fast or slow response. For example, HHL was always lower for the fast responses than the slow responses, as inflow reaches sewer systems much quicker than infiltration, causing it to have a shorter

hydrograph recession time. Each of these parameters were first calibrated manually for the initial portion of the study, then calibrated automatically using Bayesian Optimization later on.

Error Criteria

To calibrate the parameters effectively, standard error criteria were developed for each model. The two types of error calculated were percent error and absolute value percent error. Percent error is the observed value subtracted from the modeled value, divided by the observed value. Absolute value percent error simply takes the absolute value of the percent error value.

For each type of percent error, the peak flow error as well as event volume error were evaluated. Peak flow error refers to the difference between the maximum flow value seen during a storm event in the observed flow time series and the corresponding model flow time series. Event volume error refers to the difference in total volume of flow that a sewer experiences between the observed flow time series and corresponding model flow time series during a flow event.

Percent error assists in understanding the bias of the model; a negative percent error indicates the model is under predicting flow while a positive percent error indicates the model is over predicting flow. It's extremely helpful in the calibration of various capture fraction parameters such as RD and RW_{max} in the two-level streamflow models. The equations for percent error are as follows:

$$Peak\ Flow\ Percent\ Error = \frac{(PF_M - PF_O)}{PF_O} * 100 \quad (16)$$

and

$$Event\ Volume\ Percent\ Error = \frac{(EV_M - EV_O)}{EV_O} * 100, \quad (17)$$

where

PF_M = Peak flow of modeled storm event [L^3/T],

PF_O = Peak flow of observed storm event [L^3/T],

EV_M = Event volume of modeled storm event [L^3],

EV_O = Event volume of observed storm event [L^3].

Absolute value percent error assists in understanding the magnitude of error a model is exhibiting. This makes it helpful in the calibration of nearly all calibratable parameters, as it's a general indicator of a model's proficiency. The equations for absolute value percent error are as follows:

$$Peak\ Flow\ Absolute\ Value\ Percent\ Error = \left|\frac{(PF_M - PF_O)}{PF_O}\right| * 100 \quad (18)$$

and

$$Event\ Volume\ Absolute\ Value\ Percent\ Error = \left|\frac{(EV_M - EV_O)}{EV_O}\right| * 100. \quad (19)$$

Using H2Ometrics, the rainfall volumes for every storm present in the five years of historical sewer flow data were calculated. The top 15 storm events ranked by rainfall volume were then exported to Excel, where the peak flow error and event volume error were calculated for each storm using the two types of percent error. This created four error values for each of the top 15 storms, which were subsequently averaged to create two percent error and two absolute value percent error values for each model. Parameter calibration was mostly focused on the minimization of the average absolute percent error. This is because the average absolute value percent error is more representative of the magnitude of error as opposed to the bias of the

model. For instance, an average percent error of zero may seem excellent; however, the model could have an average absolute value percent error of 60%. If half of the top 15 storms have a percent error of 60% and the other half have a percent error of -60%, the model is overestimating as often as it is underestimating. While this is useful information, average absolute value percent error of the top 15 storms is more representative of the model's general proficiency.

Bayesian Optimization Using MATLAB

After a period of lengthy manual calibration, Bayesian optimization was employed to automate the calibration process. MATLAB code was written by ChatGPT after it was prompted with "Can you write sample MATLAB code that opens a connection to an Excel spreadsheet, sets input cell A7 equal to 15.3, tells Excel to recalculate, and finally retrieves the result of the calculation, which is a numeric value, from cell D23 and stores it in a MATLAB variable?" (OpenAI, 2023). Appendix B displays the raw output from ChatGPT when provided with this prompt. The code ChatGPT provided utilized the command Actxserver in MATLAB. Actxserver allows for the creation of an ongoing connection between MATLAB and Excel, allowing MATLAB to write values to specified cells of an Excel-based spreadsheet and read the value of a specified cell, whose value is reported back to MATLAB. This connection allowed the Bayesian optimization algorithm to edit specified calibratable parameters of an Excel based model and report the new error value back to MATLAB. The algorithm runs for as many trials as the user specifies; however, the default number of 30 trials was left unchanged.

Bayesian Optimization is able to optimize four parameters at a time; larger sets of parameters (>4) strain the algorithm. Therefore, for each three-level model, first the cold SHCF and hot SHCF for both the fast and slow response were optimized simultaneously, followed by the RD for fast and slow. For each two-level model, the RD and RW_{max} for the both the fast and

slow responses were optimized simultaneously. The algorithm greatly helped in finding new optimal values for many calibratable parameters, especially the cold SHCF and hot SCHF parameters used in the temperature-based AMM and the three-level streamflow models. The Bayesian Optimization algorithm requires ranges to be specified for each of the parameters it attempts to optimize. These ranges were determined by taking the final values determined through manual calibration and assigning a range of ±50% of the value.

The Bayesian Optimization algorithm goal was set to minimize the value of the average absolute value percent error of the top 15 storms in each model. However, there were two values to minimize, the average absolute value percent error of the peak flow and event volume error. The process was made more efficient by only providing one value for the algorithm to minimize. The top 15 storm event's average absolute value percent error of peak flow and event volume were averaged, and the algorithm was set to minimize this value. This allowed the algorithm to optimize the parameters with an equal bias towards either minimizing peak flow error or event volume error. The combined error value will be referred to as absolute peak and volume percent error hereinafter.

Results and Discussion

The results of the models utilizing streamflow signals were promising and displayed comparable accuracy to their temperature-based AMM counterparts. Some streamflow-based models even showed higher accuracy than their temperature-based AMM counterparts. The parameters utilized in sewer MS0453 and MS0456's models (four models per sewer) are listed in Table 1 and 2, respectively. The largest RDI/I event of each sewer, as well as an example of compounding RDI/I events, are displayed for each model in Figures 12 through 27 (two figures per model). Figures 12 through 19 display sewer MS0453's observed flow plotted against

modeled flow, while Figures 20 through 27 display the same for sewer MS0456. Analyzing the largest RDI/I event allows for the model's ability to estimate peak flows and event volumes to be evaluated while the series of compounding RDI/I events give insight regarding each model's ability to account for increasing antecedent moisture conditions. While sewer MS0456's largest RDI/I event could also represent a series of compounding RDI/I events, MS0456's models still have corresponding figures for the chosen series of RDI/I events. This decision allowed for comparison between the two sewers' corresponding models over the same time period.

Sewer MS0453

Table 1

Parameters Used in Models for Sewer MS0453

Parameters \ Model	Temp-based AMM		Milwaukee river 2-level		Milwaukee river 3-level		Lincoln creek 3-level	
	Fast Response	Slow Response	Fast Response	Slow Response	Fast Response	Slow Response	Fast Response	Slow Response
RD	0.010	0.008	0.015	0.010	0.010	0.008	0.015	0.008
RW_{max}	0.043	0.058	0.025	0.025	0.061	0.064	0.007	0.039
HHL (hrs)	11.5	48	11.5	48	11.5	48	11.5	48
AMHL (hrs)	5	24			5	24	5	24
PAT (hrs)	6	24	6	24	5	24	5	24
TAT (hrs)	168	168						
SFAT (hrs)			168	336	168	336	168	336
Hot SHCF	0.031	0.016			0.028	0.016	0.029	0.128
Cold SHCF	0.904	0.791			0.904	0.706	0.040	0.168

Figure 12

Temperature-based AMM Model of Sewer MS0453 - Largest RDI/I Event

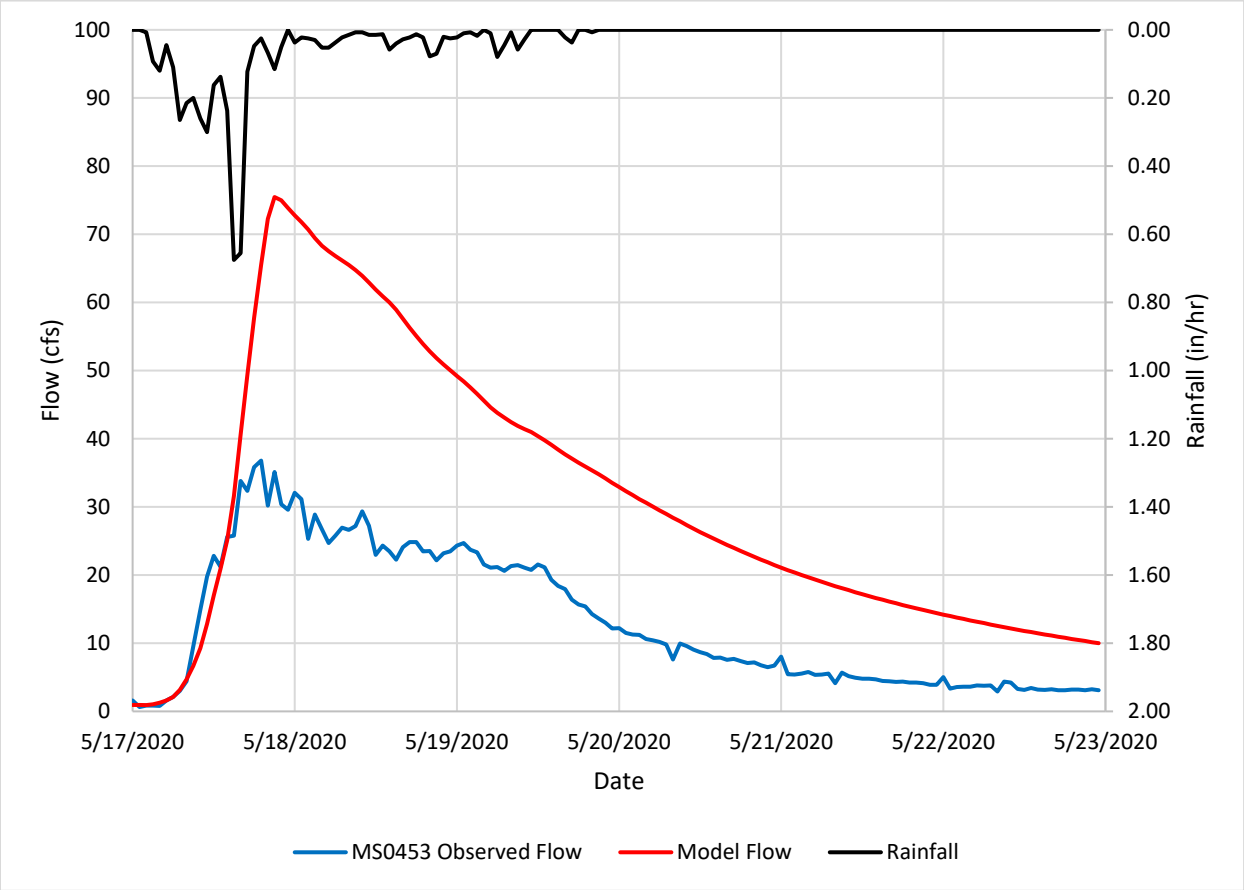

Note. The model substantially overpredicted the event in peak flow as well as volume.

Figure 13

Temperature-based AMM Model of Sewer MS0453 - Compounding RDI/I Events

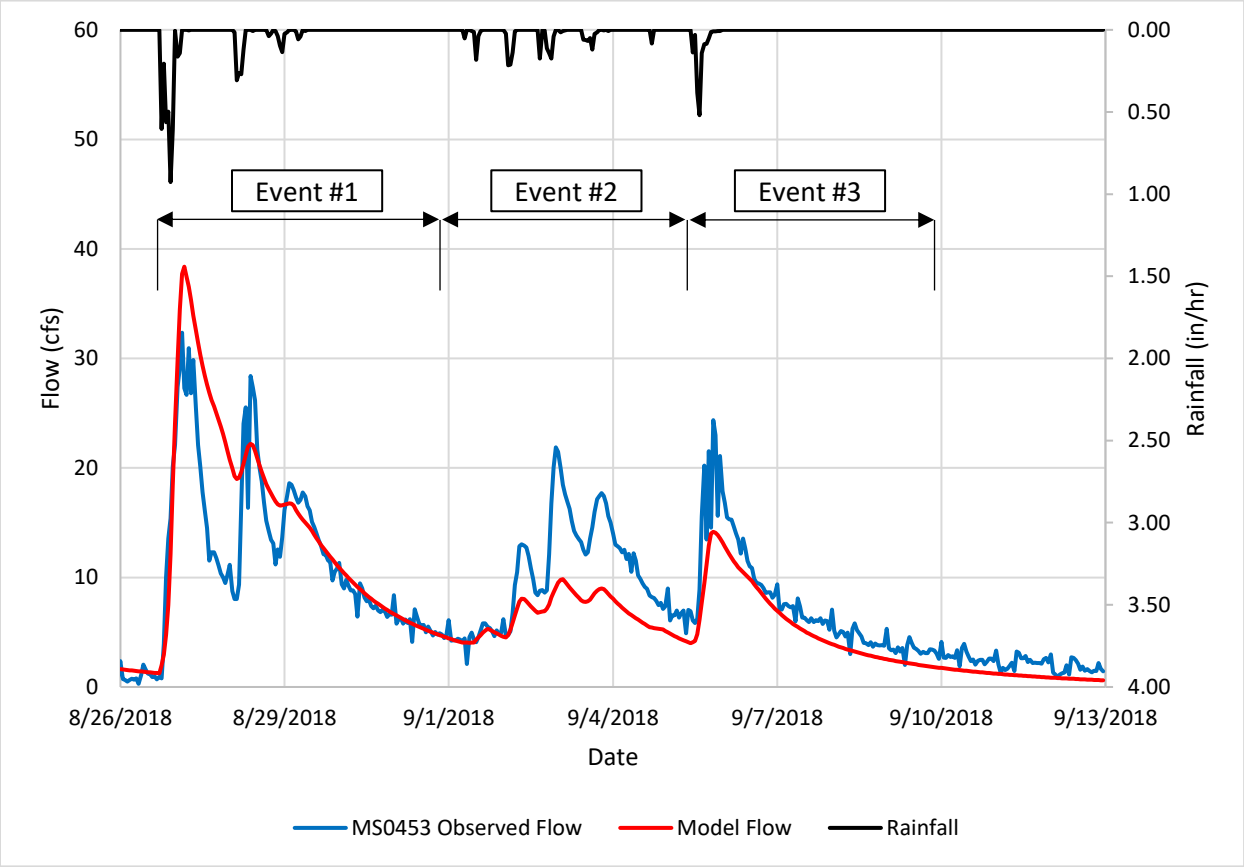

Note. The model slightly overpredicted the peak flow of Event #1. Interestingly, it underpredicts the succeeding events, Events #2 and #3.

Figure 14

Two-level Model of Sewer MS0453 Utilizing the Milwaukee River Signal - Largest RDI/I Event

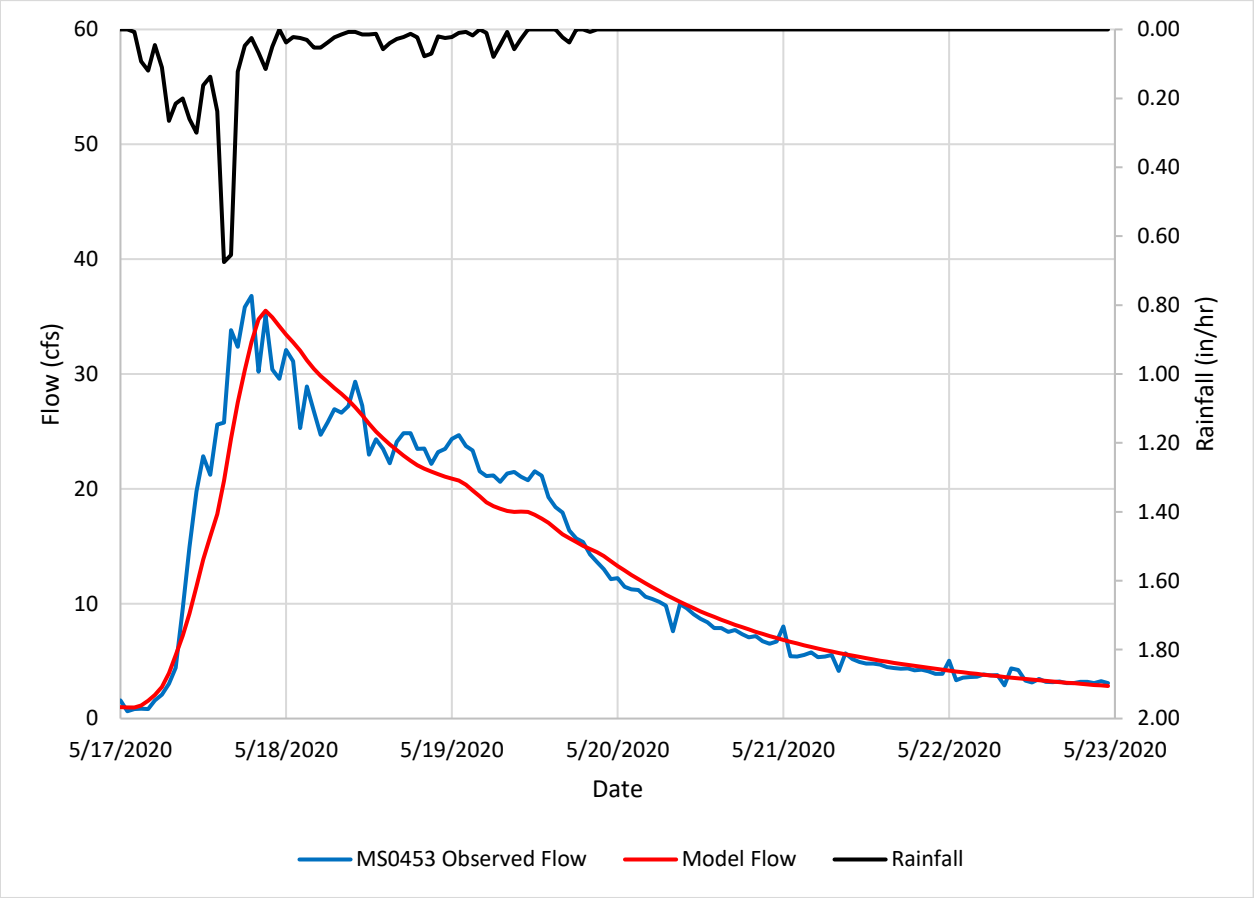

Note. The model predicted the event accurately in peak flow and volume.

Figure 15

Two-level Model of Sewer MS0453 Utilizing the Milwaukee River Signal – Compounding RDI/I Events

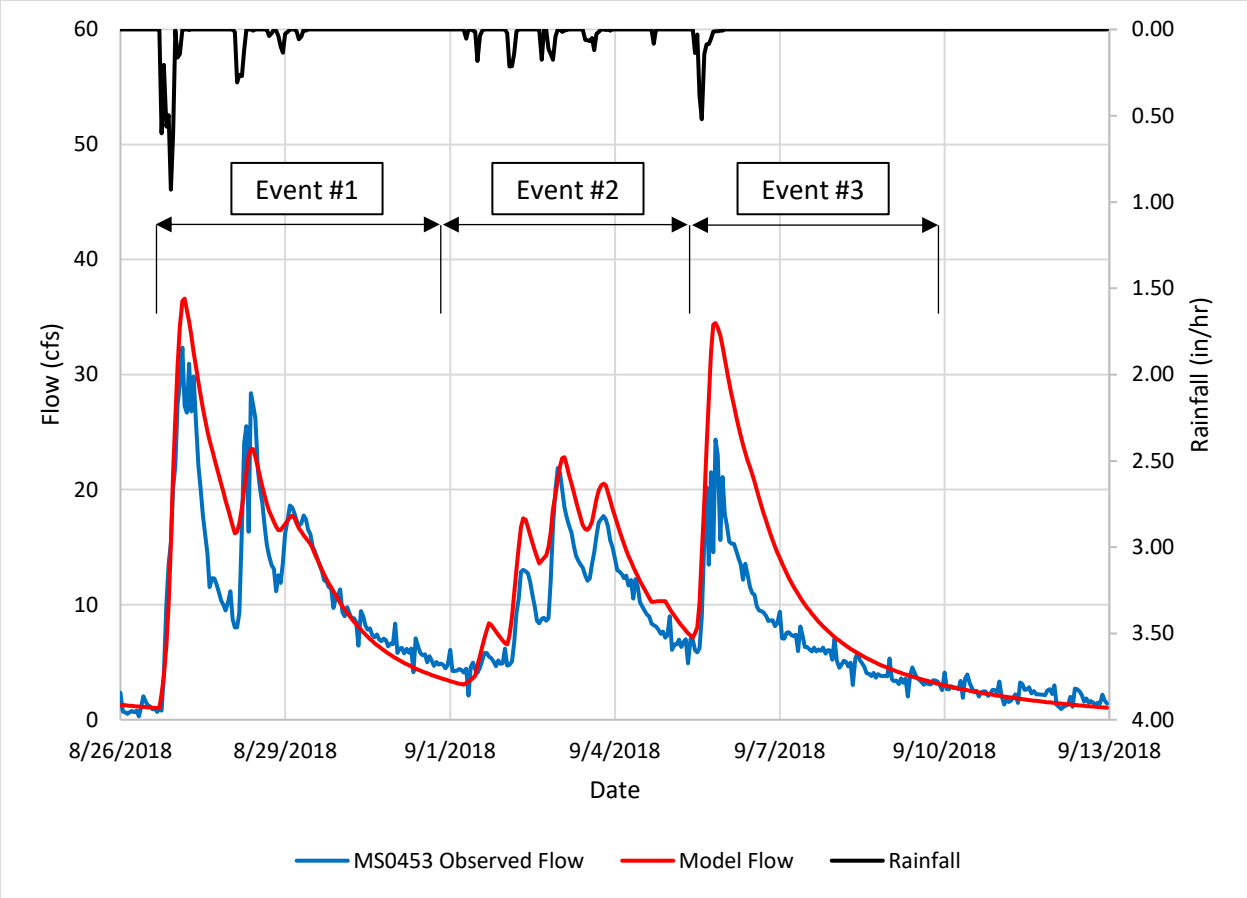

Note. The model accurately predicted Event #1 and #2. However, Event #3 was overpredicted by the model.

Figure 16

Three-level Model of Sewer MS0453 Utilizing the Milwaukee River Signal - Largest RDI/I Event

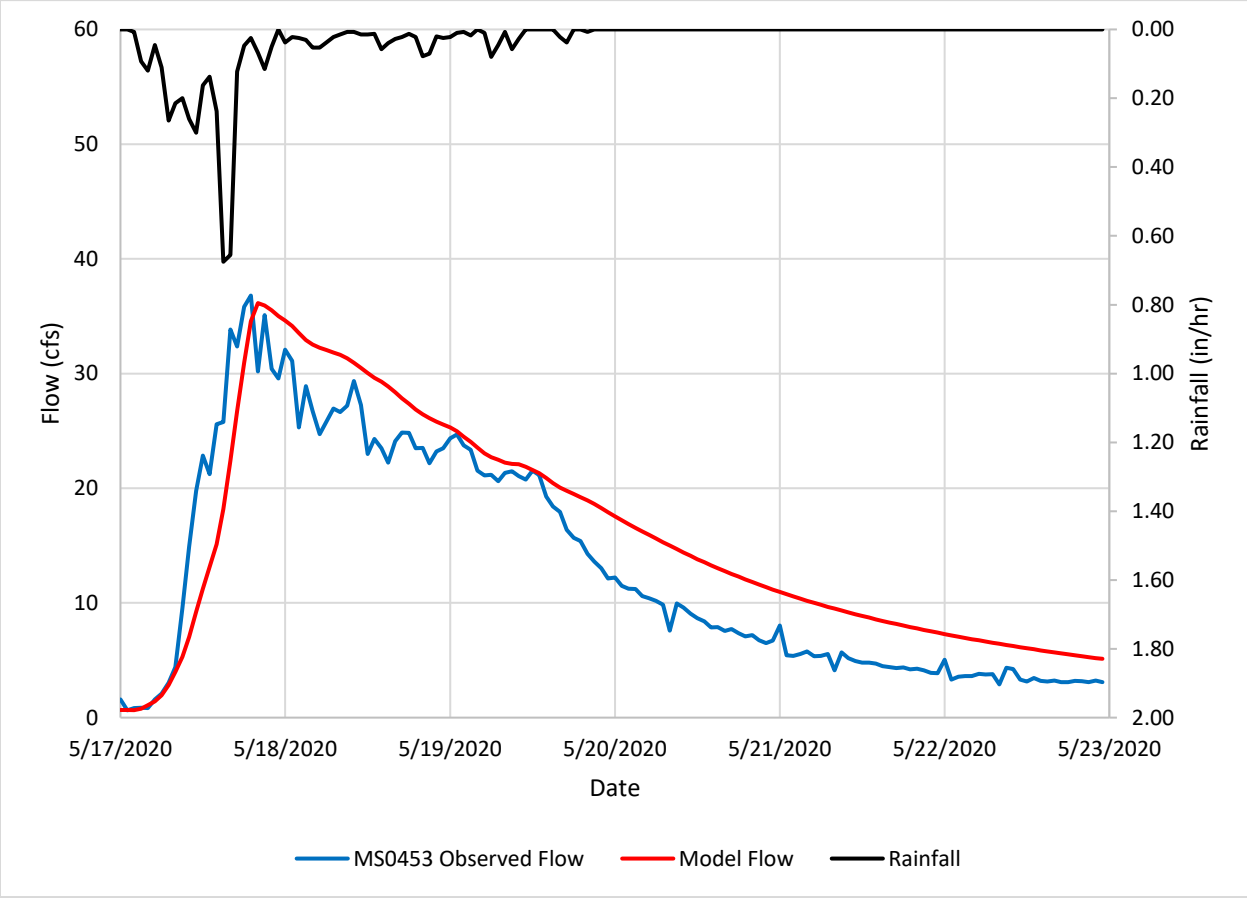

Note. The model predicted the event accurately in peak flow and volume.

Figure 17

Three-level Model of Sewer MS0453 Utilizing the Milwaukee River Signal - Compounding RDI/I Events

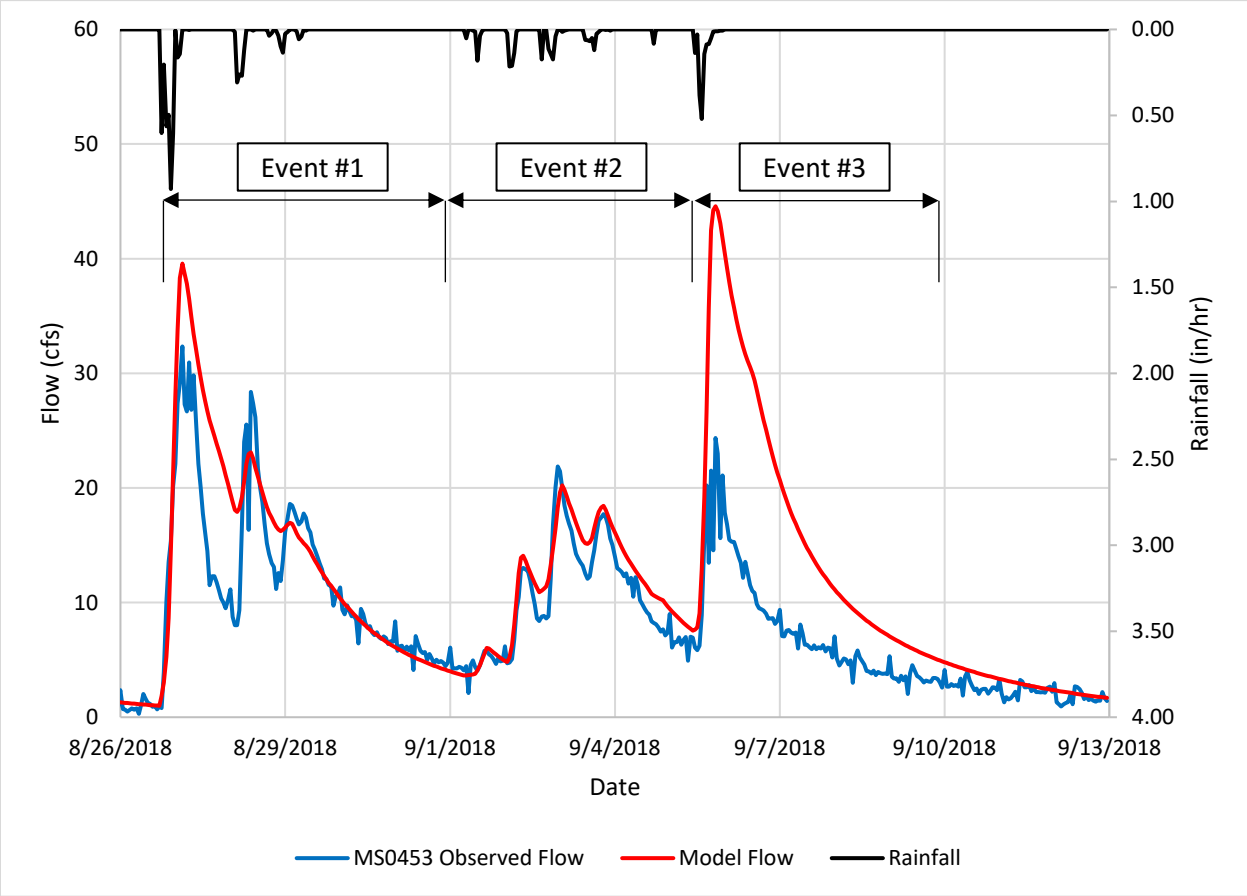

Note. The model slightly overpredicted peak flow for Event #1 while it accurately predicted Event #2's peak flow. Event #3's peak flow is overpredicted substantially. The volumes of Event #1 and #2 were predicted accurately while Event #3's volume was overpredicted.

Figure 18

Three-level Model of Sewer MS0453 Utilizing the Lincoln Creek Signal - Largest RDI/I Event

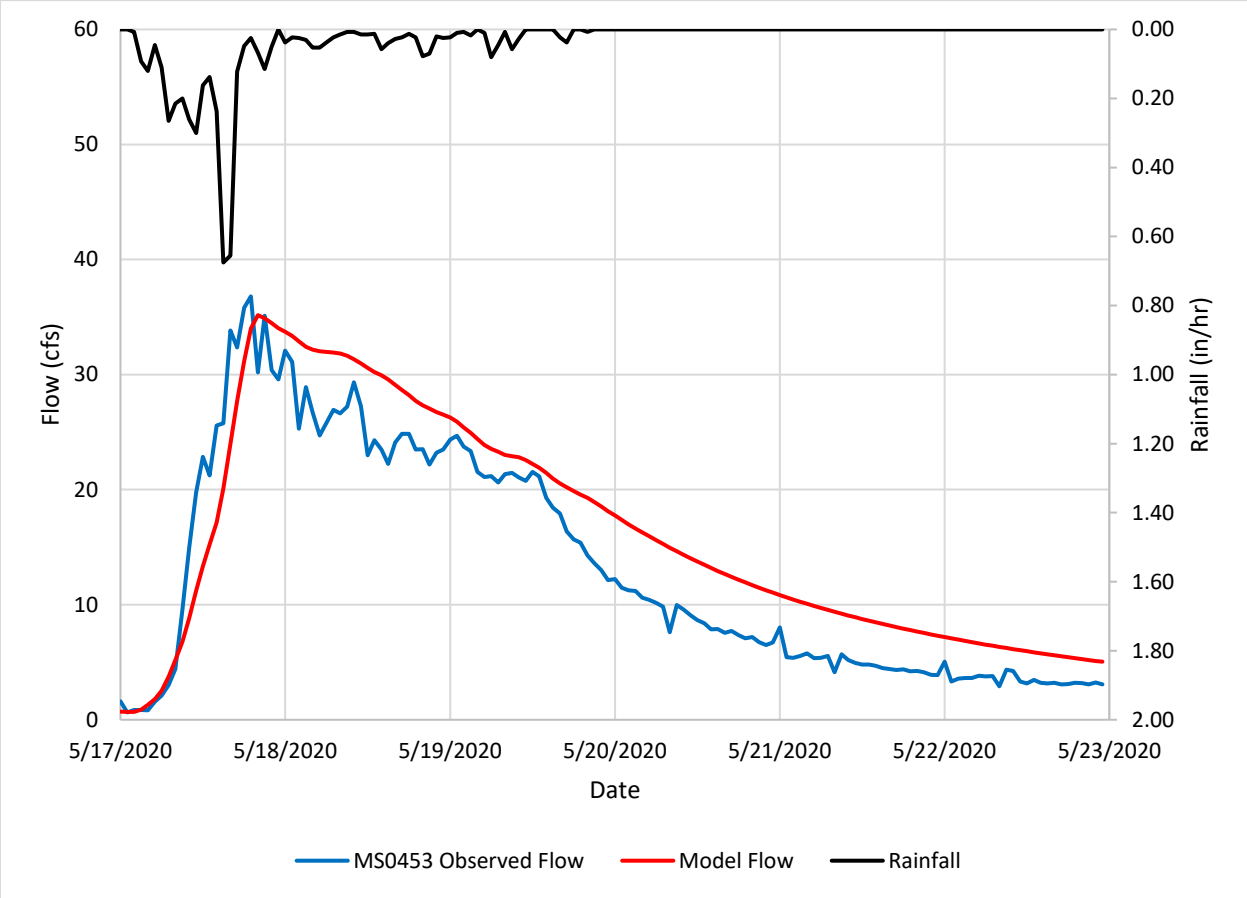

Note. The model accurately predicted the peak flow while it slightly overpredicted the volume.

Figure 19

Three-level Model of Sewer MS0453 Utilizing the Lincoln Creek Signal - Compounding RDI/I Events

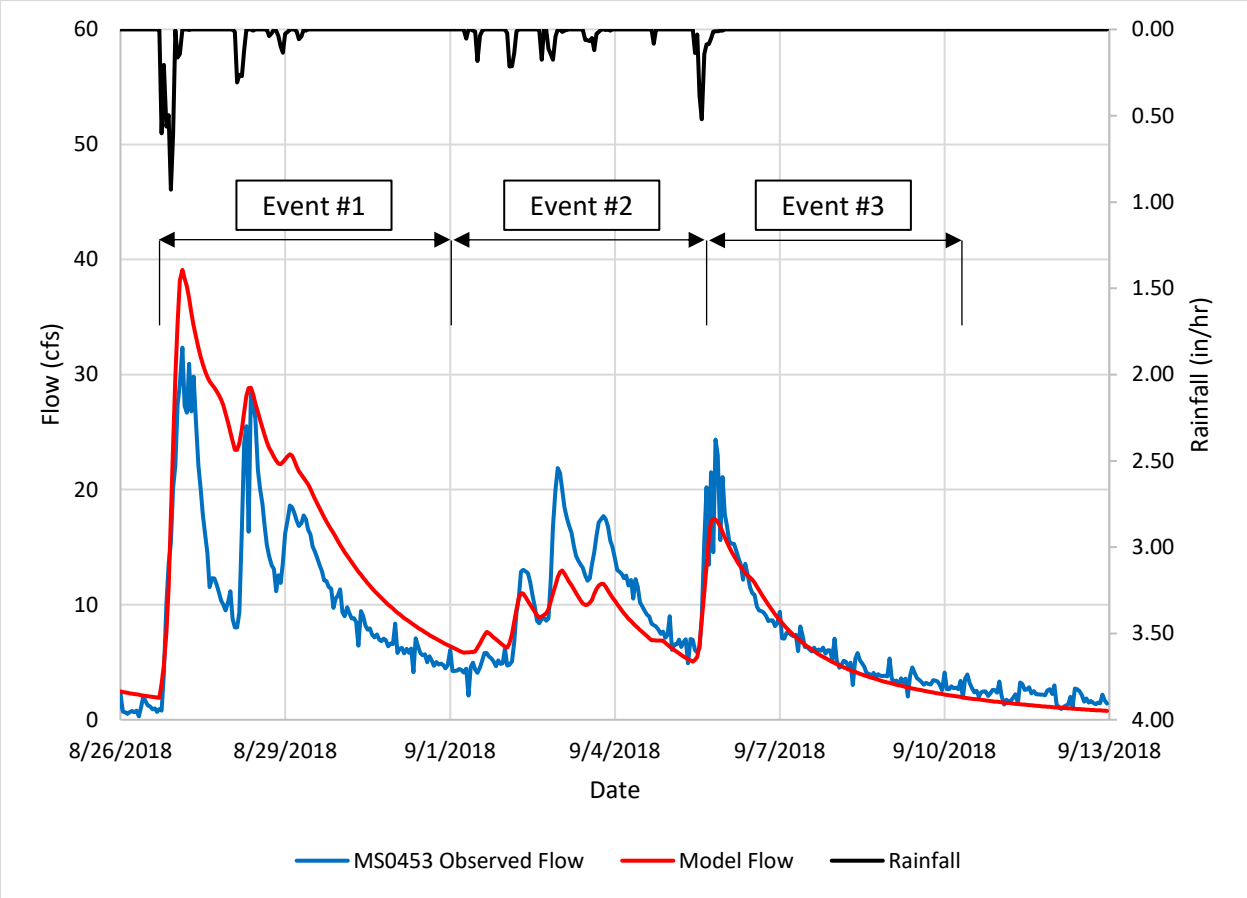

Note. The model slightly overpredicts Event #1 in peak flow and volume while it underpredicted Events #2 and #3.

Sewer MS0456

Table 2

Parameters Used in Models for Sewer MS0456

Parameters \ Model	Temp-based AMM		Milwaukee river 2-level		Lincoln creek 2-level		Lincoln creek 3-level	
	Fast Response	Slow Response	Fast Response	Slow Response	Fast Response	Slow Response	Fast Response	Slow Response
RD	0.060	0.045	0.050	0.040	0.055	0.030	0.070	0.045
RW_{max}	0.145	0.218	0.175	0.125	0.090	0.060	0.003	0.012
HHL (hrs)	5	24	5	24	5	24	5	24
AMHL (hrs)	2	24					2	36
PAT (hrs)	5	24	6	24	6	24	6	24
TAT (hrs)	168	168						
SFAT (hrs)			168	336	168	336	168	336
Hot SHCF	0.120	0.038					0.028	0.033
Cold SHCF	4.110	2.164					0.032	0.076

Figure 20

Temperature-based AMM Model of Sewer MS0456 - Largest RDI/I Event

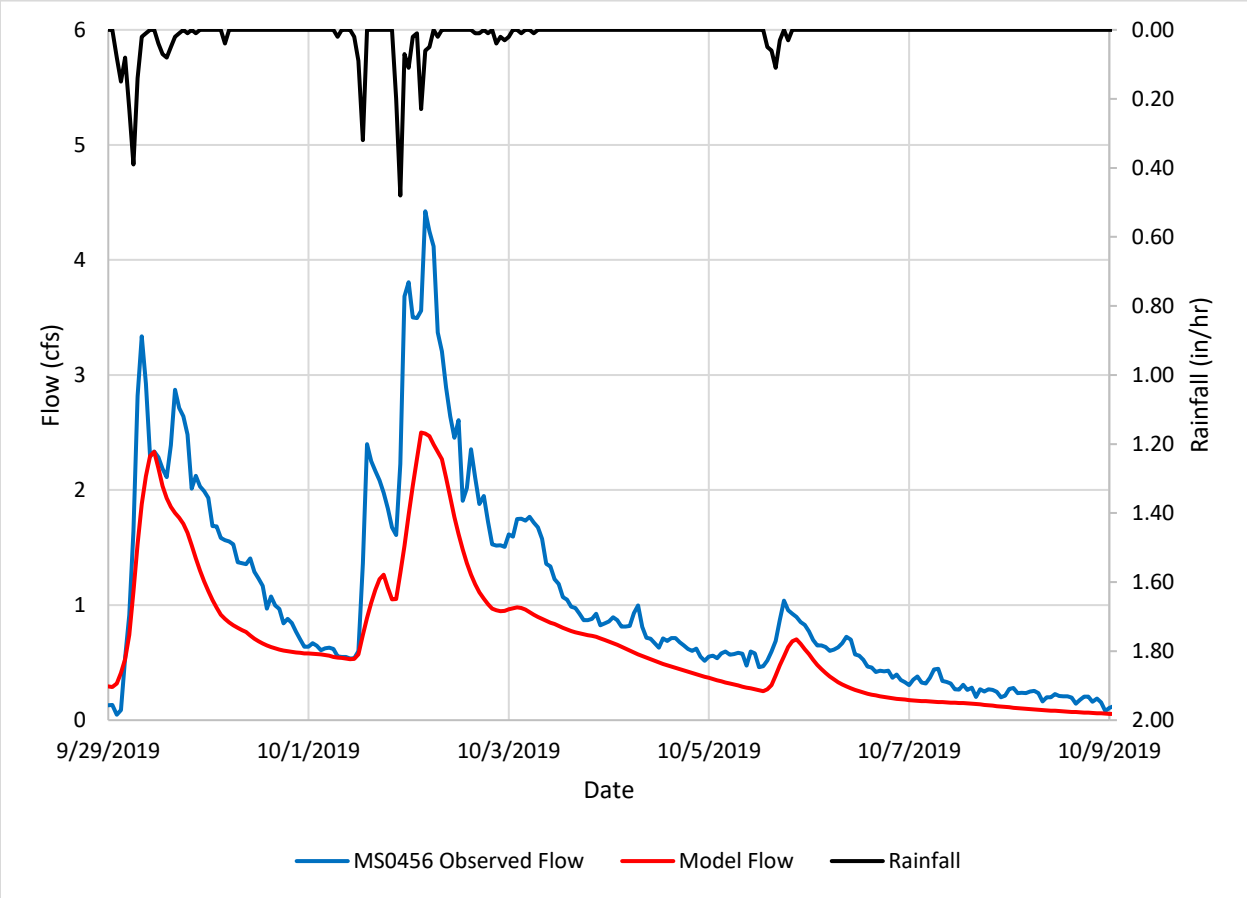

Note. The model underpredicted the peak flow of the event as well as the volume.

Figure 21

Temperature-based AMM Model of Sewer MS0456 - Compounding RDI/I Events

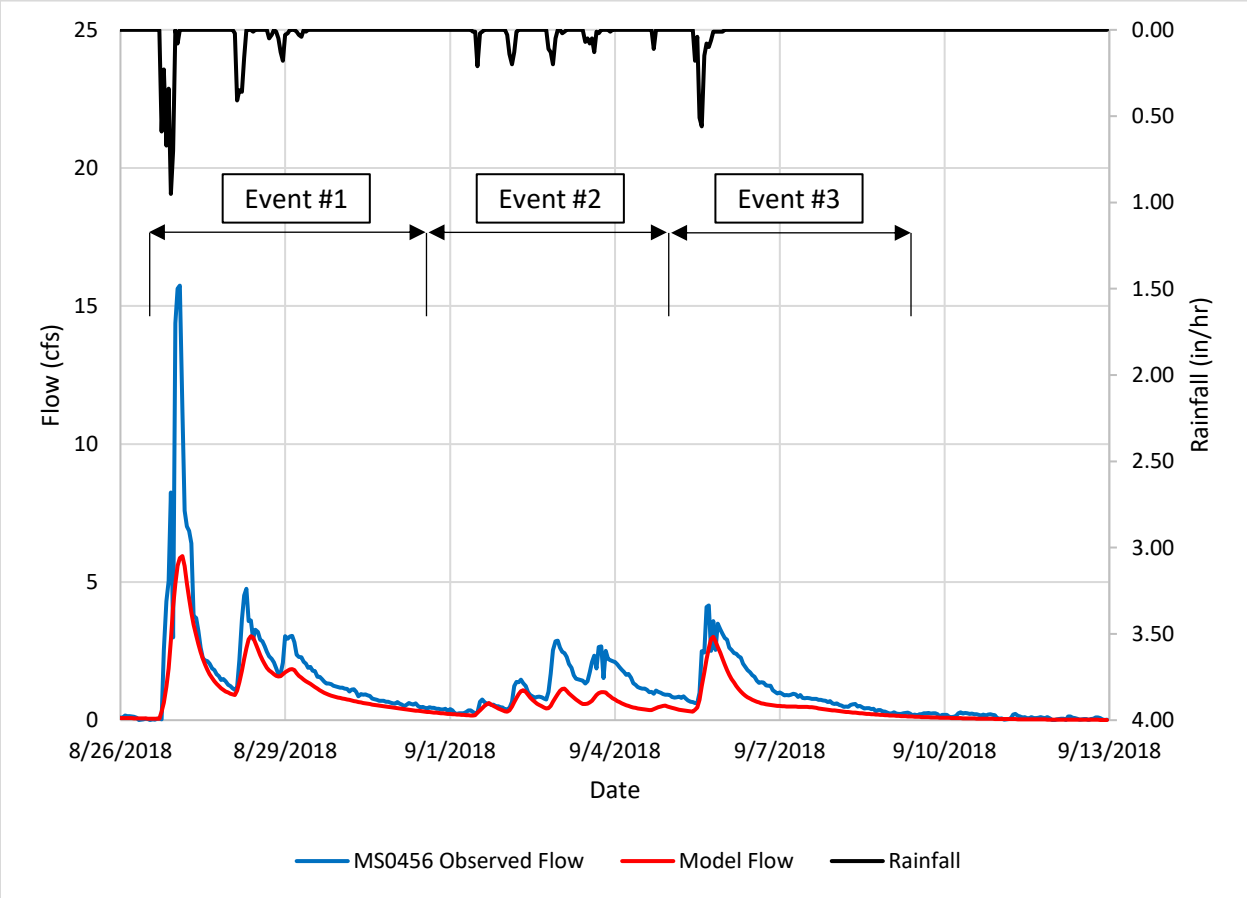

Note. The model substantially underpredicted the peak flow of Event #1 as well as the peak flows of Event #2. Peak flow of Event #3 was predicted accurately by the model. The volume of each event was slightly underpredicted by the model.

Figure 22

Two-level Model of Sewer MS0456 Utilizing the Milwaukee River Signal - Largest RDI/I Event

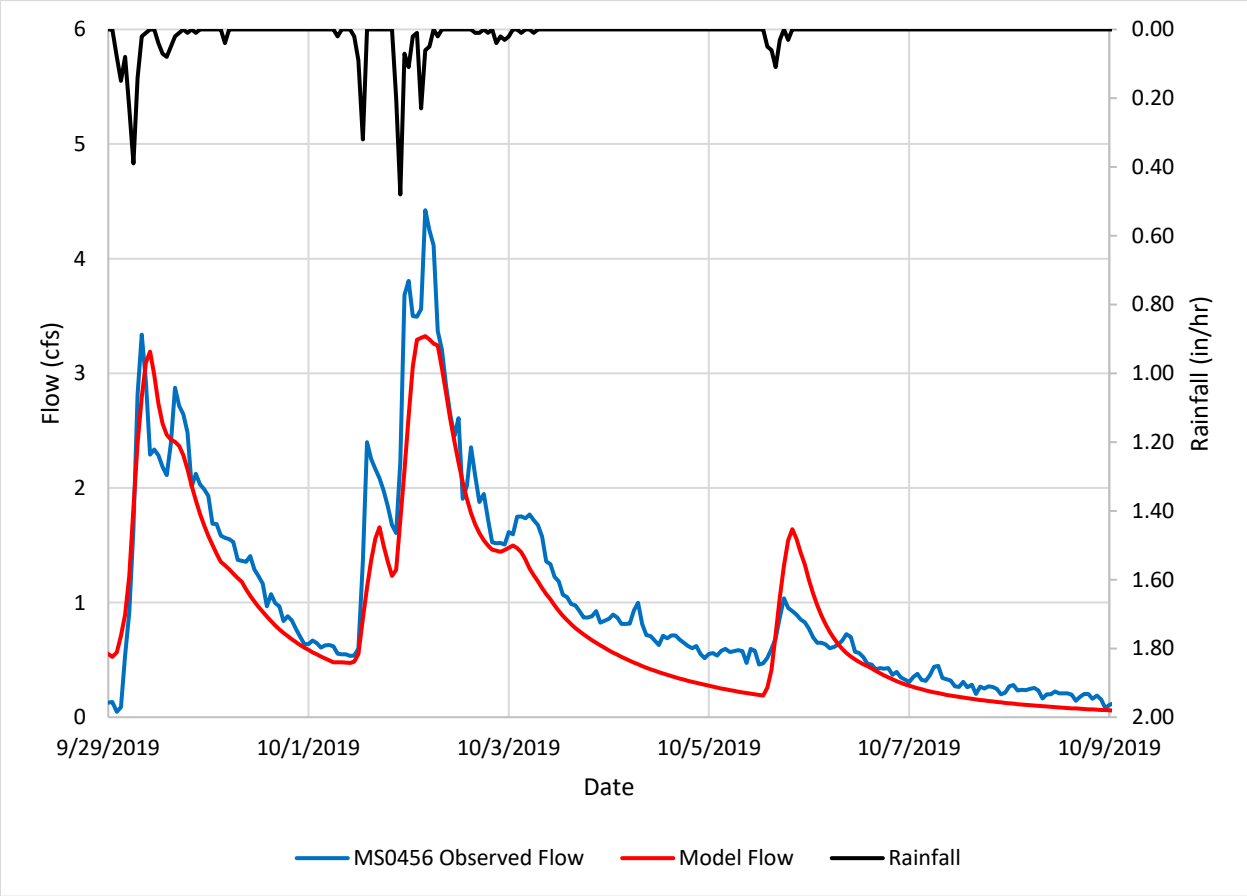

Note. The model accurately predicted the peak flow of the event as well as the volume.

Figure 23

Two-level Model of Sewer MS0456 Utilizing the Milwaukee River Signal - Compounding RDI/I Events

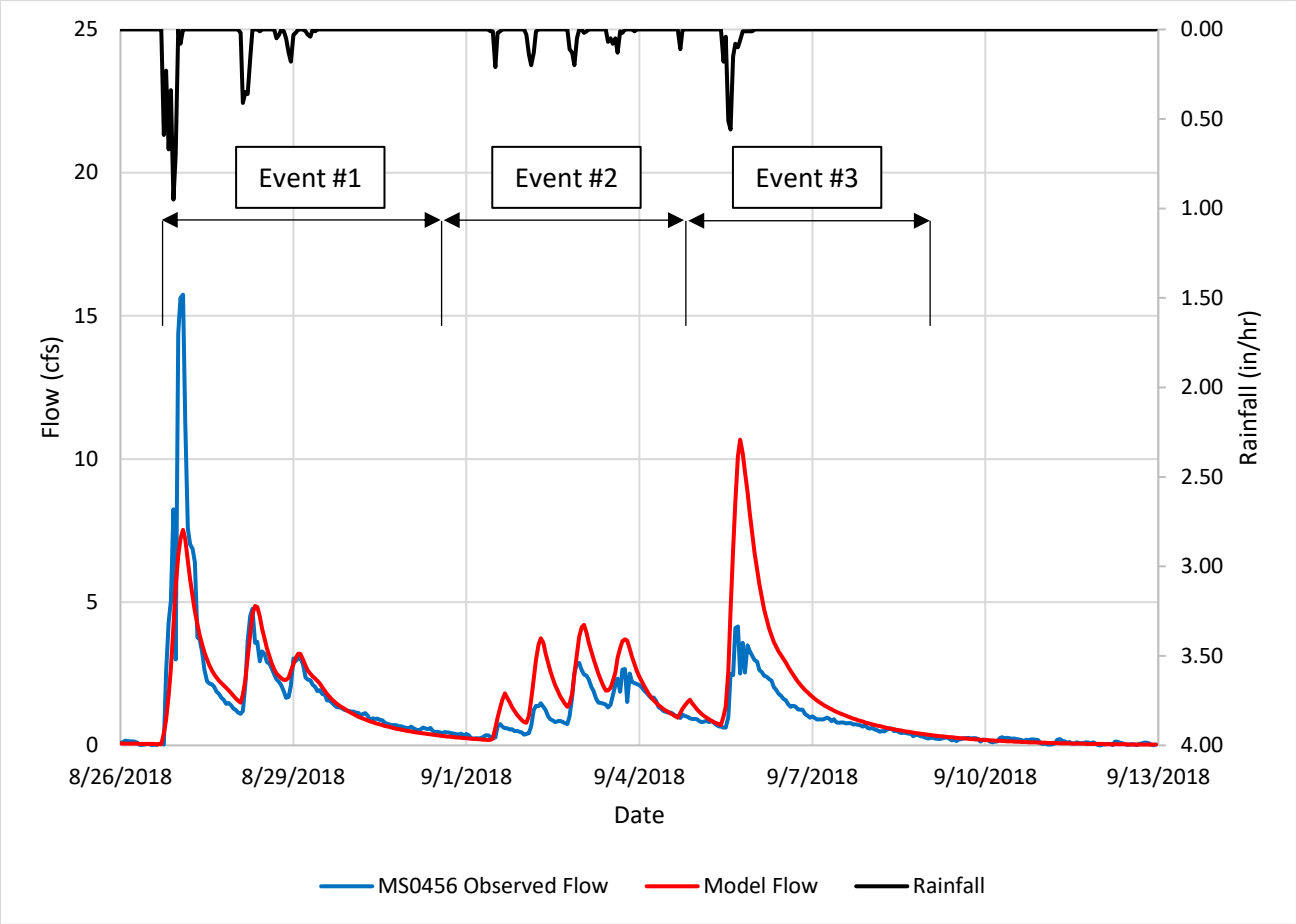

Note. The model substantially underpredicted the peak flow of Event #1 while it accurately predicted the volume. Event #2 and #3 were overpredicted by the model in both peak flow and volume.

Figure 24

Two-level Model of Sewer MS0456 Utilizing the Lincoln Creek Signal - Largest RDI/I Event

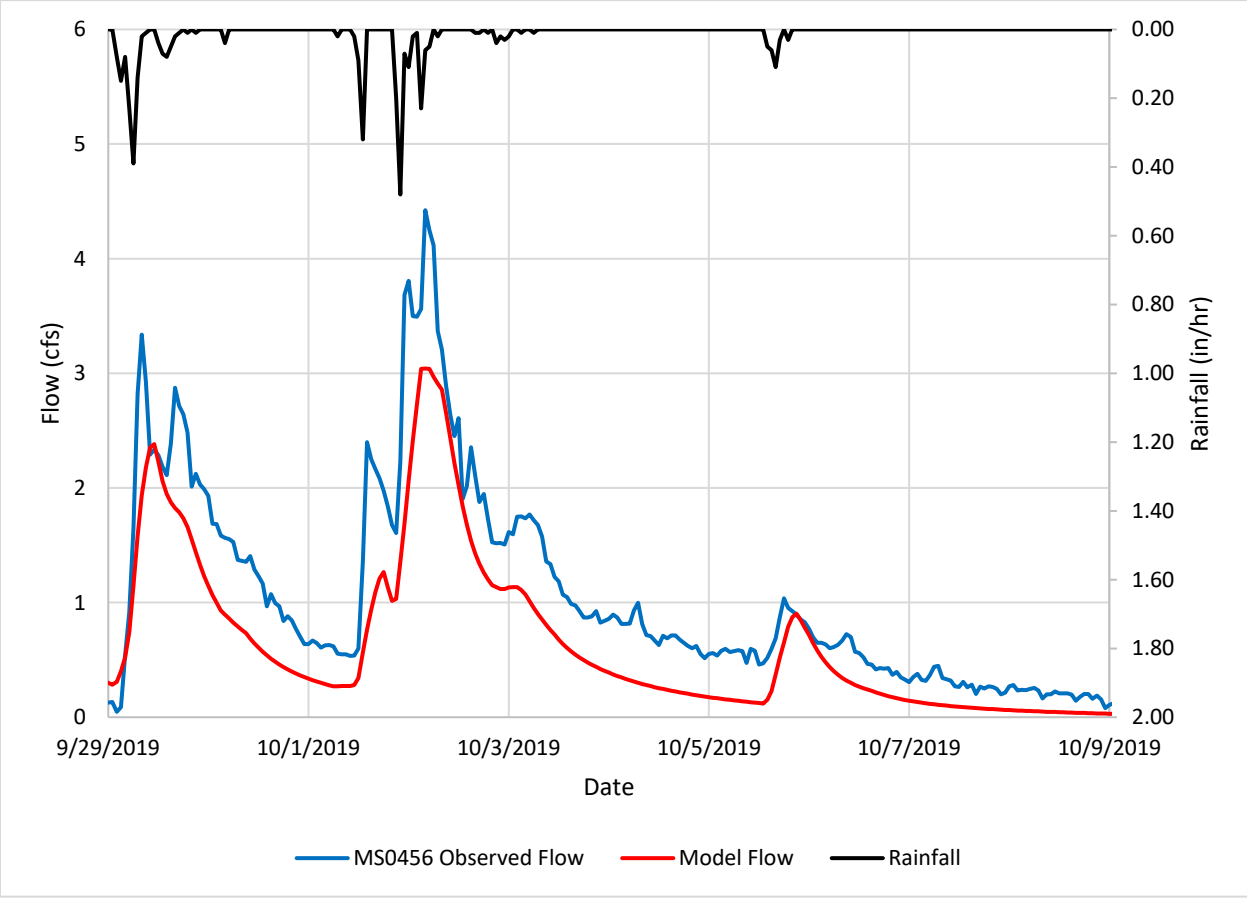

Note. The model slightly underestimated the peak flow and volume of the event.

Figure 25

Two-level Model of Sewer MS0456 Utilizing the Lincoln Creek Signal - Compounding RDI/I Events

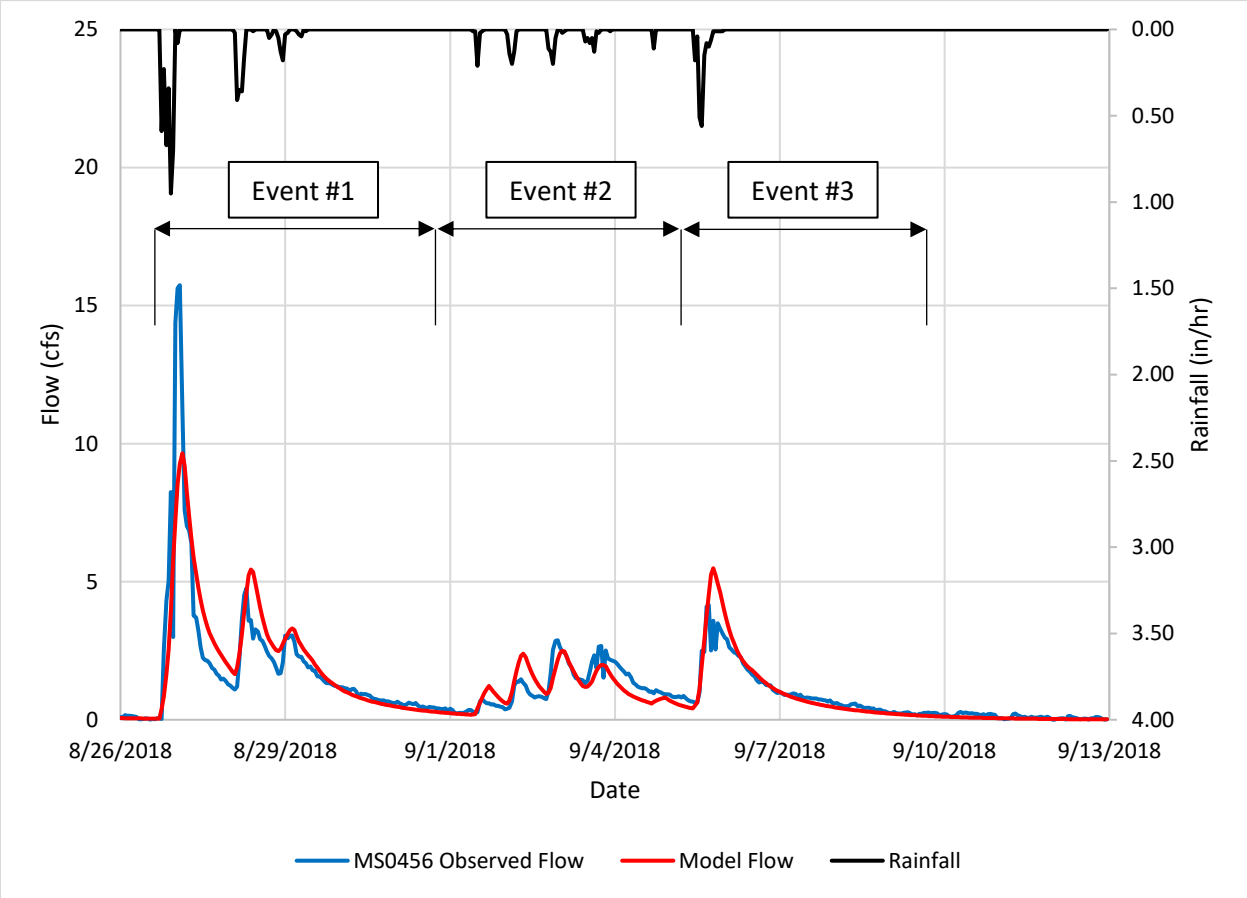

Note. The model underpredicted Event #1's peak flow while accurately predicting its volume. The peak flow and volume of Events #2 and #3 were accurately predicted.

Figure 26

Three-level Model of Sewer MS0456 Utilizing the Lincoln Creek Signal - Largest RDI/I Event

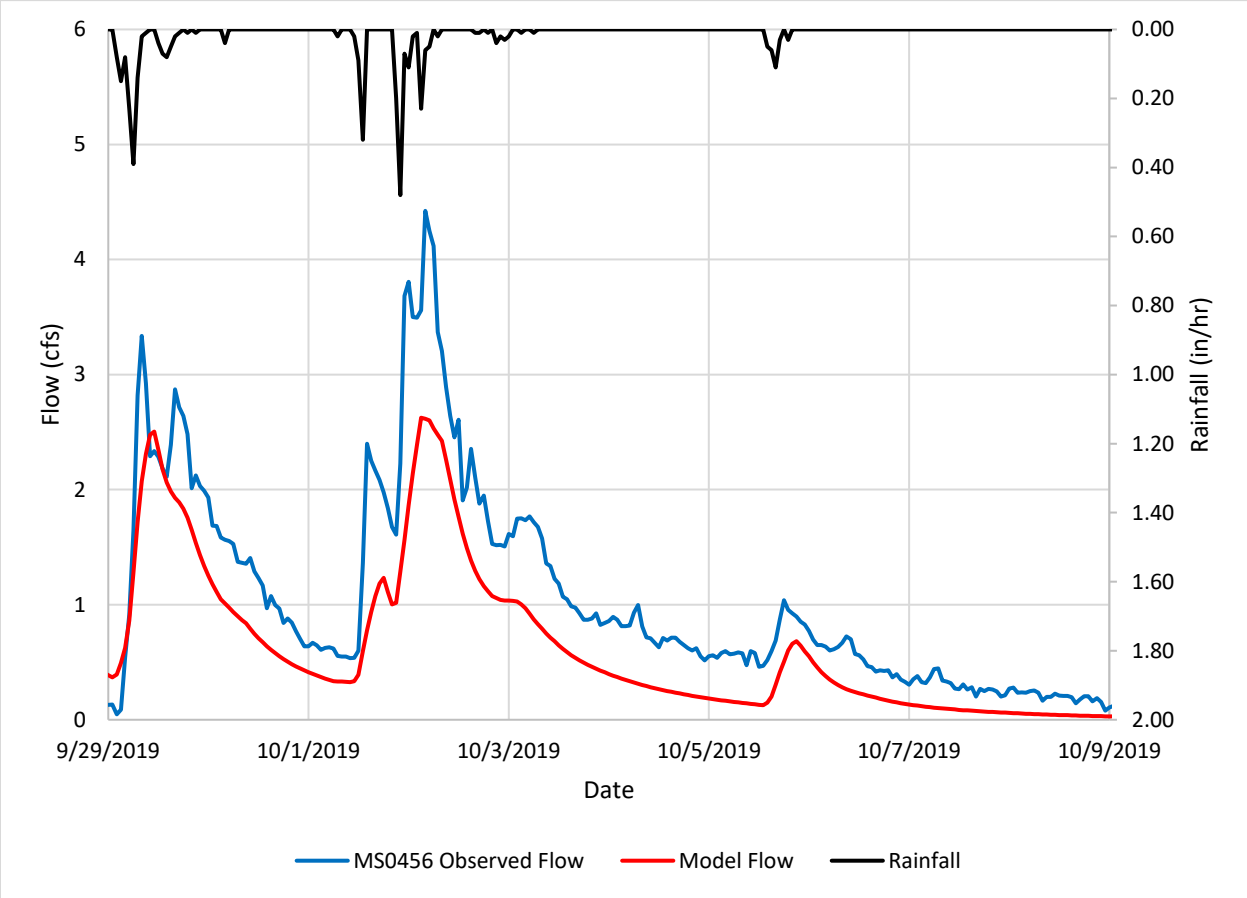

Note. The model substantially underestimated the peak flow and slightly underestimated the volume of the event.

Figure 27

Three-level Model of Sewer MS0456 Utilizing the Lincoln Creek Signal - Compounding RDI/I Events

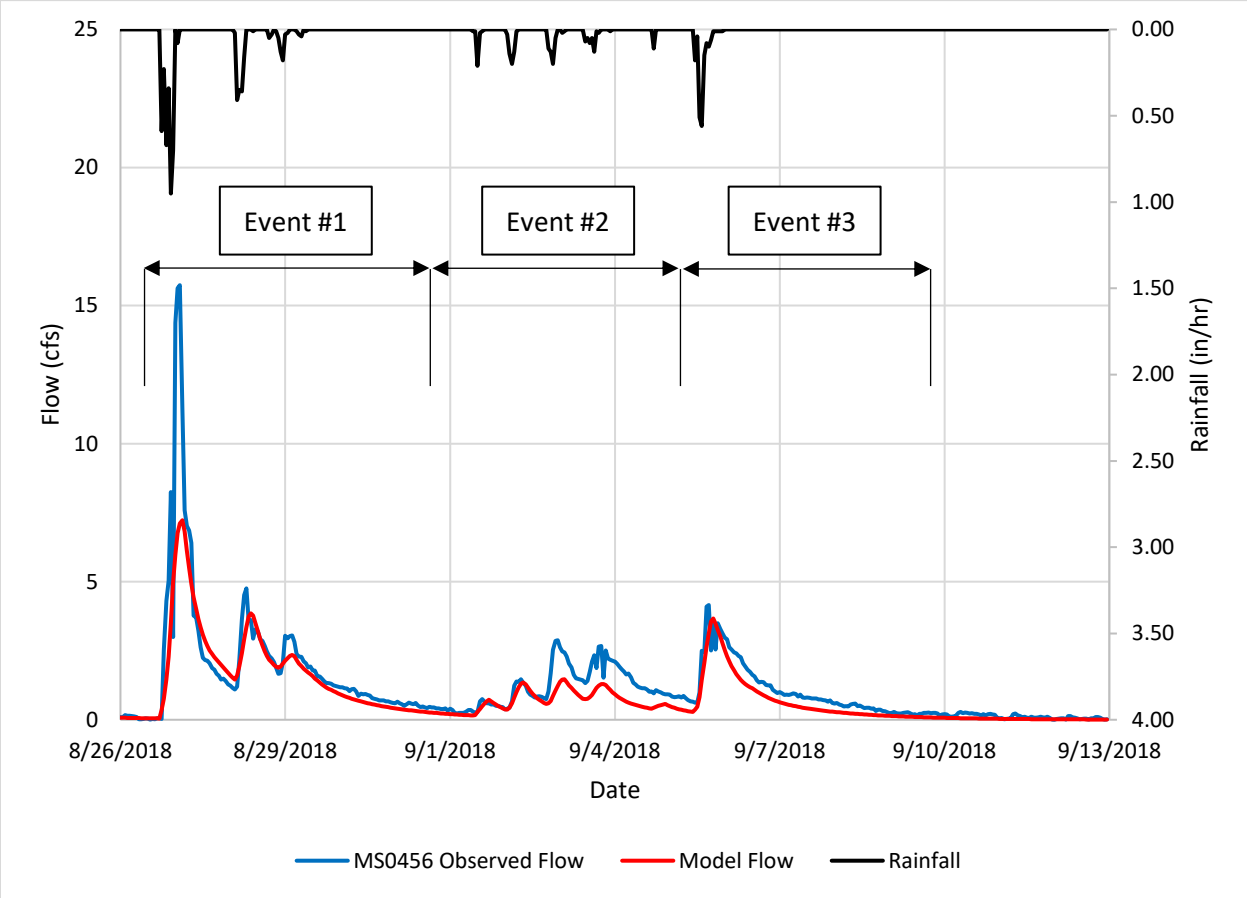

Note. The model substantially underpredicted the peak flow and slightly underpredicted the volume of Event #1 and #2. Peak flow of Event #3 was predicted accurately by the model.

Sewer MS0453's models have much lower capture fraction parameters than sewer MS0456's models. This was expected due to their catchment areas differing in land use, with MS0453's catchment area being more rural than urban as opposed to MS0456, which is mostly urban. Because of the impervious areas within MS0456's catchment, rainfall is less likely to be absorbed by the soil, increasing its fast response RD and RW_{max} capture fractions. MS0456 being

more urban also appears to have resulted in its fast response AMHL parameter being lower than MS0453's (two hours compared to five hours). The lower the AMHL, the quicker the system dries. Antecedent moisture has an increased effect on MS0453 as it retains antecedent moisture longer than MS0456. This assertation is further reinforced by MS0453 having larger HHLs than MS0456 for both responses. MS0453 appears to receive roughly equal amounts of RDI/I from inflow and infiltration sources while MS0456 receives RDI/I primarily from inflow sources, which increase and decrease quickly.

The PAT parameter for every model was nearly identical, with fast responses ranging from a PAT of five to six hours, and slow responses staying constant at 24 hours. The PAT influences the time between rainfall and an RDI/I response in the sewer. Because of the PAT's uniformity across every model, it may be representative of a larger area than the two sewers' catchments.

The Cold and Hot SHCF parameters for the models are largely dependent on the type of model utilized. Temperature-based models and models utilizing the Milwaukee River signal appear to have similar Cold and Hot SHCF ranges. The aforementioned model types have Cold and Hot SHCF values that vary by about one order of magnitude. However, models utilizing the Lincoln Creek signal appear to have much smaller Cold and Hot SHCF ranges, with their Cold and Hot SHCFs being nearly identical. As a result, Lincoln Creek's signal influences its model's flow by nearly the same amount regardless of its magnitude. This means that Lincoln Creek's flow is less influenced by antecedent moisture conditions, producing similar responses to rainfall events regardless of antecedent moisture conditions. This was expected, as Lincoln Creek resides in a highly urban area with large amounts of impervious area.

Conversely, the Milwaukee River's signal is a strong indicator of antecedent moisture conditions. This was expected, as it is a regional river that has influenced areas alongside it to remain less developed. The Milwaukee River's shores are home to many nature preserves, thereby reducing impervious areas within its watershed. The fact that the Cold and Hot SHCF parameters for both temperature-based models and models utilizing the Milwaukee River signal are extremely similar indicates that the Milwaukee River's flow is influenced by antecedent moisture conditions.

The Milwaukee River signal is able to represent antecedent moisture conditions to the same level of accuracy as a temperature signal, if not better. In Figure 12, the temperature-based model severely overpredicted the peak flow and volume of the RDI/I event, while in Figure 14, the event was modeled accurately. The cause of overprediction in Figure 12 lies in the temperature signal utilized by the model. The temperature ranged between 49 to 51 F° during the event, resulting in the temperature-based model calculating an RW of 0.041 and 0.031 at the event's peak for its fast and slow response, respectively. In Figure 14, the three-level model utilizing the Milwaukee River signal's scaled $MASF^3_t$ value ranged between 60 to 65 F° during the event's time period. At the event's peak, the three-level model calculated an RW of 0.004 and 0.026 for its fast and slow response, respectively, much lower than the temperature-based model. Because the three-level Milwaukee River model produces a lower capture fraction, the RDI/I event was modeled with higher accuracy than the temperature-based model. In this event, the Milwaukee River signal was a better representation of antecedent moisture conditions than the temperature signal. Figure 28 compares the RW values for each model throughout the duration of the RDI/I event.

Figure 28

Comparison of the Temperature-based AMM and Three-level Milwaukee River RW Values During Sewer MS0453's Largest RDI/I Event

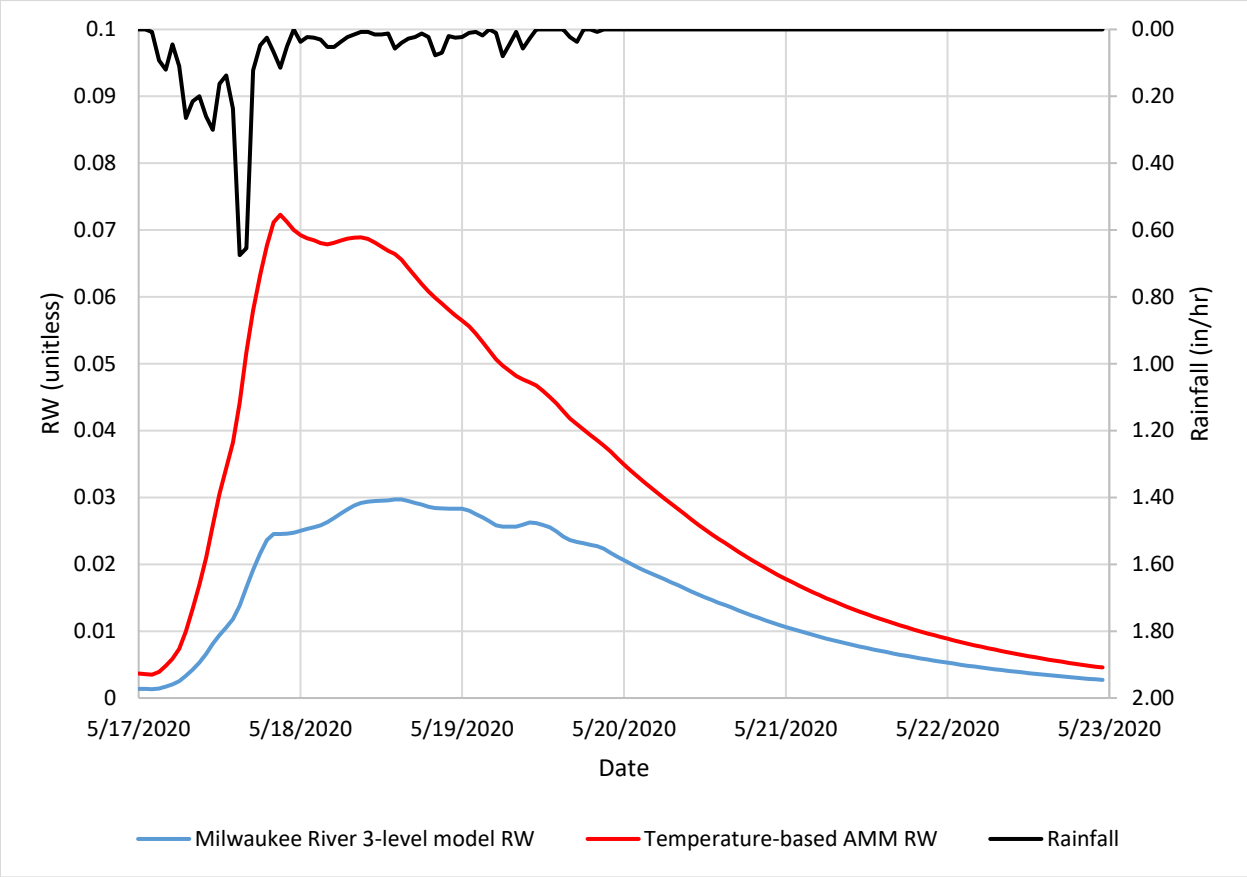

Note. The temperature-based AMM method substantially overpredicts the RW value during the RDI/I event for sewer MS0453.

The error values that guided the calibration of each parameter are listed in Table 3.

Table 3

Error Values Employed in Parameter Calibration

Sewer	Model	Peak Event Percent Error	Event Volume Percent Error	Absolute Peak and Volume Percent Error
MS0453	Temperature-based AMM	40%	45%	43%
	Milwaukee River two-level model	26%	32%	29%
	Milwaukee River three-level model	34%	36%	35%
	Lincoln Creek three-level model	35%	51%	43%
MS0456	Temperature-based AMM	25%	29%	27%
	Milwaukee River two-level model	25%	31%	28%
	Lincoln Creek two-level model	34%	39%	37%
	Lincoln Creek three-level model	30%	38%	34%

Note. The peak event and event volume percent errors displayed in Table 3 represent the average of the 15 absolute value percent error values acquired via the top 15 storms for each corresponding model. The absolute peak and volume percent errors displayed represent the average of each model's peak event and event volume percent error.

Figure 29 compares the absolute peak and volume percent error between each sewer's corresponding model in a horizontal bar graph.

Figure 29

Absolute Peak and Volume Percent Error Comparison

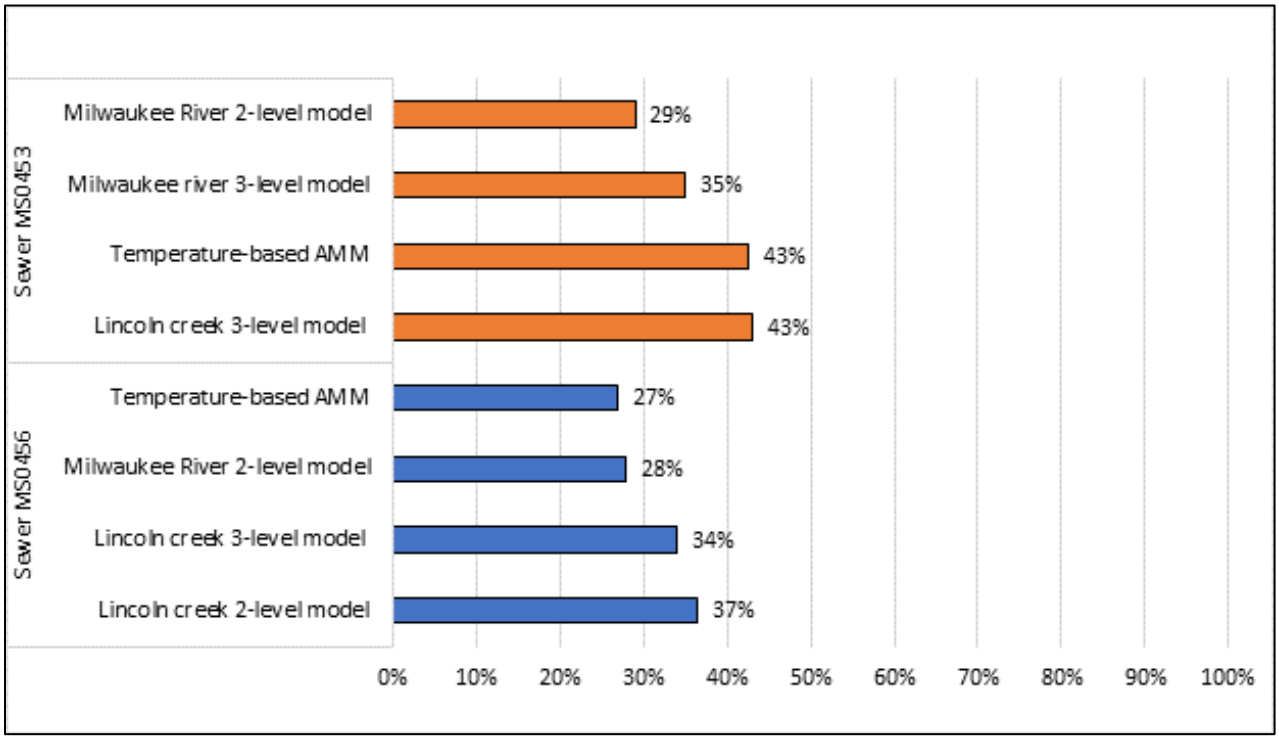

Sewer MS0453's two-level and three-level models utilizing the Milwaukee River signal outperformed its corresponding temperature-based AMM model. Sewer MS0456's temperature-based AMM model slightly outperformed its corresponding two-level model using the Milwaukee River signal, but only by 1%. Two-level and three-level models using the Lincoln Creek signal performed adequately but were outperformed by models using both temperature and Milwaukee River signals. This was expected as Lincoln Creek is not as strong of an indicator of antecedent moisture conditions due to its urban location, as stated previously in this section.

The results of this study have provided insight regarding the use of a streamflow signal to represent the antecedent moisture conditions of a sewer's catchment area. The streamflow

signals in two-level and three-level models produced comparable or better results than the standard temperature-based AMM models.

Sewer MS0453 and MS0456's two-level models using the Milwaukee River signal achieved the lowest error amongst all other streamflow-based models. There are two potential reasons why the two-level models outperformed their three-level counterparts. First, the two-level models did not scale the streamflow signal to a corresponding temperature value. Instead, the third level of AMM was excluded from the model's calculations and RW_{max} was multiplied by the scaled $MASF^2_t$ value directly. The scaled $MASF^2_t$ value directly influences the RW_{max} parameter in two-level models as opposed to the less direct influence of the RW_{t-1} parameter via the SHCF in three-level models. Giving the streamflow signal a more direct path of influence in two-level models could have given two-level models an edge over three-level models. Second, two-level models have fewer parameters associated with their calibration due to their exclusion of the third level of AMM. Two-level models have only four calibratable parameters as opposed to the three-level models, which have six calibratable parameters. Fewer calibratable parameters simplifies the calibration process and could have allowed the Bayesian Optimization algorithm to determine more accurate parameters for two-level models.

A key factor that may have influenced each model's accuracy is the variability of rainfall distribution. During the summer, rainfall depths can change drastically over short distances (W. Gonwa, personal communication, May 10, 2023). Variability of rainfall distribution between a sewer's catchment area and its representative rain gage would result in the sewer's models inaccurately predicting the RDI/I response. For example, the compounding RDI/I events depicted for each of sewer MS0456's models underpredict Event #1's peak flow. MS0456's representative rain gage, WS1224, likely experienced variability in rainfall and recorded a lower

depth than what MS0456's catchment area experienced. The compounding RDI/I events occurred during late summer, increasing the possibility of rainfall variability.

Conclusion

Streamflow gages were able to accurately represent the antecedent moisture conditions of a nearby sewer's catchment area. The implementation of a streamflow signal in antecedent moisture modeling produced comparable or better results than the standard temperature-based AMM approach. The use of streamflow signals of large regional rivers are recommended, as models using the Milwaukee River's signal achieved higher accuracy than models using Lincoln Creek's signal. Accurately predicting wet weather flow in sanitary sewer systems is imperative in the design of strategies that limit the environmental and public health impacts of SSO's and increased WWTP loads. The results of this study support an opinion that further research into the use of streamflow signals to represent antecedent moisture conditions would be beneficial for the field of sanitary sewer system modeling.

Recommendations

The data collected for this study were specific to the Milwaukee area. In order to verify the results presented, further research should be conducted analyzing data from different regions with different climates than that of Milwaukee, WI. The ability of a streamflow signal to represent the antecedent moisture conditions of a sanitary sewer system may change depending on the location's climate. Additionally, future research should include a larger sample size of sewer systems in order to confirm the results of this study.

Attempting to model five years of sanitary sewer flow may have increased the difficulty of achieving accurate results. It's possible that certain parameters used in the various sewer

models may have changed slightly over the duration of the data. A shorter duration of time may provide a more accurate representation of the sanitary sewer system's parameters, thereby increasing the accuracy of the model's RDI/I flow prediction.

Future studies should address the variability of rain. The installation of rain gages in the center of sewers' catchments areas would provide a more accurate estimation of the total RDI/I volume the sewer experiences.

References

Black & Veatch. (1999). *Optimization of Collection System Maintenance Frequencies and System.* ASCE, EPA Cooperative Agreement #CX 824902-01-0.

Cretu, G., Nagy, C., & Boncia, F. (2005). *Chapter 2 Watershed Characteristics.* Retrieved from Virtual Campus in Hydrology and Water Resources: https://echo2.epfl.ch/VICAIRE/mod_1a/chapt_2/text.htm#:~:text=The%20shape%20of%20a%20watershed,and%20it%20generates%20higher%20flow.

Czachorski, R. (2010, January 1). *H2Ometrics*. Retrieved from H2Ometrics: https://h2ometrics.com/

Czachorski, R., Edgren, D., Gonwa, W., & Morgan, E. (2022, May 26). *AMM users conference.* Retrieved from H2Ometrics: https://h2ometrics.com/amm-users-conference-2022/

De Feo, G., Antoniou, G., Fardin, H. F., El-Gohary, F., Zheng, X. Y., Reklaityte, I., . . . Yannopoulos, S. a. (2014). The historical development of sewers worldwide. *Sustainability*, *6*(6), 3936-3974. https://doi.org/10.3390/su6063936

Edgren, D., Czachorski, R., & Gonwa, W. (2023). Reparameterizing the antecedent moisture model. *[Manuscript submitted for publication]*.

Hayes, A. (2022, March 1). *Bayes' Theorem: What it is, the formula, and examples*. Retrieved from Investopedia: https://www.investopedia.com/terms/b/bayes-theorem.asp#:~:text=Bayes'%20Theorem%20states%20that%20the,probability%20of%20the%20first%20event.

Lai, F.-h. (2008). *Review of sewer design criteria and RDII prediction methods.* U.S. Environmental Protection Agency, Washington D.C. Retrieved from https://nepis.epa.gov/Exe/ZyNET.exe/P1008BP3.TXT?ZyActionD=ZyDocument&Client=EPA&Index=2006+Thru+2010&Docs=&Query=&Time=&EndTime=&SearchMethod=1&TocRestrict=n&Toc=&TocEntry=&QField=&QFieldYear=&QFieldMonth=&QFieldDay=&IntQFieldOp=0&ExtQFieldOp=0&XmlQuery=

NCEI. (n.d.). *Climate Data Online*. Retrieved 2023, from NOAA National Centers for Environmental Information: https://www.ncdc.noaa.gov/cdo-web/

Office of Water Programs. (2008). *Impacts of sanitary sewer overflows and combined sewer overflows on human health and on the environment: a literature review.* California State University Sacremento.

OpenAI. (2023). *ChatGPT* (March 21 version) [Large Language Model]. https://chat.openai.com/chat

Rödel, S., Günthert, F. W., & Brüggemann, T. (2017). Investigating the impacts of extraneous water on wastewater treatment plants. *Water Science and Technology, 75*(3-4), 847-855. https://doi.org/https://doi.org/10.2166/wst.2016.570

Sola, K. J., Bjerkholt, J. T., & Lindholm, O. G. (2020). Analysing consequences of infiltration and inflow water (I/I-water) using cost-benefit analyses. *Water science and technology, 82*(7), 1312-1326. https://doi.org/https://doi.org/10.2166/wst.2020.395

United States Geological Survey. (n.d.). *USGS*. Retrieved from StreamStats: https://streamstats.usgs.gov/ss/

USGS. (n.d.). *USGS water data for the nation*. Retrieved 2022, from United States Geological Survey.

Van Pelt, T., & Czachorski, R. (2002). The application of system identification to inflow and infiltration modeling and design storm event simulation for sanitary collection systems. *Proceedings of the Water Environment Federation, 2002*, 607-634. https://doi.org/10.2175/193864702784162796

Viessman, W., Lewis, G. L., & Knapp, J. W. (1989). *Introduction to hydrology.* Harpercollins College Div.

Village of Shorewood, WI. (2009, April 10). *Sanitary sewer system*. Retrieved from Village of shorewood: https://www.villageofshorewood.org/884/Sanitary-Sewer-System

Walski, T. (2021, September 3). *RTK for RDII*. Retrieved from Virtuosity: https://blog.virtuosity.com/rtk-for-rdii

WEF Collection Systems Committee. (2017). *Sanitary sewer systems: rainfall derived infiltration and inflow (RDII) modeling fact sheet*. Retrieved from Water Environment Federation: https://www.wef.org/globalassets/assets-wef/direct-download-library/public/03---resources/wsec-2017-fs-001-rdii-modeling-fact-sheet---final.pdf

Weiland, D. A. (2020). *Using system identification to model near-term wet weather sewer flow*. [Master's Thesis, Milwaukee School of Engineering (MSOE)]. MSOE Library. https://milwaukee.ipac.sirsidynix.net/ipac20/ipac.jsp?uri=full=3100001~!767415~!0

Zanoni, A. E., & Rutkowski, R. J. (1972). Per capita loadings of domestic wastewater. *Water Pollution Control Federation, 44*(9), 1756-1762. Retrieved from https://www.jstor.org/stable/25037604

Appendix A: Model Error Values

Table A1

Error Values for Two-level Model Using Milwaukee River - Sewer MS0453

			Error		Absolute Percent Error		Percent Error	
Event Rank	Start	End	Peak Event (cfs)	Event Volume (cf)	Peak Event (cfs)	Event Volume (cf)	Peak Event	Event Volume
1	5/17/2020 4:00	5/23/2020 8:00	-1.28	-2.06E+07	3%	2%	-3%	-2%
2	9/29/2019 3:00	10/10/2019 8:00	1.20	-3.99E+08	9%	19%	9%	-19%
3	8/6/2021 13:00	8/19/2021 4:00	6.43	8.49E+08	18%	52%	18%	52%
4	8/26/2018 18:00	9/1/2018 9:00	4.26	9.33E+07	13%	12%	13%	12%
5	6/18/2018 6:00	6/24/2018 8:00	-10.90	-8.03E+07	37%	15%	-37%	-15%
6	9/11/2022 5:00	9/17/2022 8:00	4.26	2.13E+08	15%	41%	15%	41%
7	4/28/2020 5:00	5/6/2020 8:00	-9.66	-9.54E+07	38%	14%	-38%	-14%
8	3/22/2022 17:00	3/28/2022 18:00	-8.11	-2.85E+08	50%	55%	-50%	-55%
9	9/29/2018 2:00	10/5/2018 7:00	-4.48	6.90E+06	23%	2%	-23%	2%
10	5/3/2021 11:00	5/13/2021 5:00	-9.49	-2.94E+08	50%	46%	-50%	-46%
11	7/9/2020 16:00	7/14/2020 3:00	4.37	1.52E+08	21%	76%	21%	76%
12	12/11/2020 3:00	12/19/2020 9:00	-6.69	-2.30E+08	49%	53%	-49%	-53%
13	4/10/2021 7:00	4/19/2021 6:00	-4.35	-1.82E+08	31%	38%	-31%	-38%
14	9/1/2018 17:00	9/5/2018 7:00	0.94	8.30E+07	4%	27%	4%	27%

Note. One of sewer MS0453's largest 15 events was omitted due to an erroneous sewer meter reading.

Therefore, only the 14 largest events were tabulated for sewer MS0453

Table A2

Error Values for Three-level Model using Milwaukee River - Sewer MS0453

			Error		Absolute Percent Error		Percent Error	
Event Rank	Start	End	Peak Event (cfs)	Event Volume (cf)	Peak Event (cfs)	Event Volume (cf)	Peak Event	Event Volume
1	5/17/2020 4:00	5/23/2020 8:00	-1.05	7.35E+07	3%	9%	-3%	9%
2	9/29/2019 3:00	10/10/2019 8:00	-2.40	-6.13E+08	19%	30%	-19%	-30%
3	8/6/2021 13:00	8/19/2021 4:00	6.43	7.80E+08	18%	48%	18%	48%
4	8/26/2018 18:00	9/1/2018 9:00	7.23	1.26E+08	22%	16%	22%	16%
5	6/18/2018 6:00	6/24/2018 8:00	-14.41	-1.47E+08	49%	-27%	-49%	27%
6	9/11/2022 5:00	9/17/2022 8:00	1.39	1.88E+08	5%	36%	5%	36%
7	4/28/2020 5:00	5/6/2020 8:00	-13.50	-2.18E+08	54%	33%	-54%	-33%
8	3/22/2022 17:00	3/28/2022 18:00	-10.78	-3.60E+08	67%	70%	-67%	-70%
9	9/29/2018 2:00	10/5/2018 7:00	-7.97	-9.51E+07	40%	21%	-40%	-21%
10	5/3/2021 11:00	5/13/2021 5:00	-12.24	-3.97E+08	65%	62%	-65%	-62%
11	7/9/2020 16:00	7/14/2020 3:00	1.81	1.37E+08	9%	68%	9%	68%
12	12/11/2020 3:00	12/19/2020 9:00	-9.02	-2.96E+08	66%	68%	-66%	-68%
13	4/10/2021 7:00	4/19/2021 6:00	-7.39	-2.71E+08	53%	56%	-53%	-56%
14	9/1/2018 17:00	9/5/2018 7:00	-1.66	3.96E+07	8%	13%	-8%	13%

Table A3

Error Values for Temperature-based AMM - Sewer MS0453

			Error		Absolute Percent Error		Percent Error	
Event Rank	Start	End	Peak Event (cfs)	Event Volume (cf)	Peak Event (cfs)	Event Volume (cf)	Peak Event	Event Volume
1	5/17/2020 4:00	5/23/2020 8:00	37.48	8.94E+08	102%	107%	102%	107%
2	9/29/2019 3:00	10/10/2019 8:00	-2.67	-7.20E+08	21%	35%	-21%	-35%
3	8/6/2021 13:00	8/19/2021 4:00	15.66	1.21E+09	44%	74%	44%	74%
4	8/26/2018 18:00	9/1/2018 9:00	5.58	6.83E+07	17%	8%	17%	8%
5	6/18/2018 6:00	6/24/2018 8:00	-14.10	-1.44E+08	48%	26%	-48%	-26%
6	9/11/2022 5:00	9/17/2022 8:00	8.63	3.64E+08	31%	71%	31%	71%
7	4/28/2020 5:00	5/6/2020 8:00	-3.38	1.96E+08	13%	30%	-13%	30%
8	3/22/2022 17:00	3/28/2022 18:00	-7.78	-2.58E+08	48%	50%	-48%	-50%
9	9/29/2018 2:00	10/5/2018 7:00	-2.69	7.41E+07	14%	16%	-14%	16%
10	5/3/2021 11:00	5/13/2021 5:00	-10.15	-3.24E+08	54%	50%	-54%	-50%
11	7/9/2020 16:00	7/14/2020 3:00	-3.35	4.17E+07	16%	21%	-16%	21%
12	12/11/2020 3:00	12/19/2020 9:00	-5.64	-1.81E+08	41%	42%	-41%	-42%
13	4/10/2021 7:00	4/19/2021 6:00	-6.26	-2.37E+08	45%	49%	-45%	-49%
14	9/1/2018 17:00	9/5/2018 7:00	-12.94	-1.39E+08	59%	46%	-59%	-46%

Table A4

Error Values for Three-level Model Using Lincoln Creek - Sewer MS0453

			Error		Absolute Percent Error		Percent Error	
Event Rank	Start	End	Peak Event (cfs)	Event Volume (cf)	Peak Event	Event Volume	Peak Event	Event Volume
1	5/17/2020 4:00	5/23/2020 8:00	-1.63	1.68E+08	4%	20%	-4%	20%
2	9/29/2019 3:00	10/10/2019 8:00	-1.35	-5.82E+08	11%	28%	-11%	-28%
3	8/6/2021 13:00	8/19/2021 4:00	17.12	2.40E+09	48%	148%	48%	148%
4	8/26/2018 18:00	9/1/2018 9:00	6.76	3.89E+08	21%	48%	21%	48%
5	6/18/2018 6:00	6/24/2018 8:00	-11.28	-1.27E+07	39%	-2%	-39%	2%
6	9/11/2022 5:00	9/17/2022 8:00	9.11	5.37E+08	33%	104%	33%	104%
7	4/28/2020 5:00	5/6/2020 8:00	-11.11	-1.12E+08	44%	17%	-44%	-17%
8	3/22/2022 17:00	3/28/2022 18:00	-9.33	-3.20E+08	58%	62%	-58%	-62%
9	9/29/2018 2:00	10/5/2018 7:00	-4.55	2.06E+07	23%	4%	-23%	4%
10	5/3/2021 11:00	5/13/2021 5:00	-10.40	-3.37E+08	55%	52%	-55%	-52%
11	7/9/2020 16:00	7/14/2020 3:00	3.59	1.93E+08	18%	96%	18%	96%
12	12/11/2020 3:00	12/19/2020 9:00	-7.46	-2.57E+08	55%	59%	-55%	-59%
13	4/10/2021 7:00	4/19/2021 6:00	-6.08	-2.48E+08	44%	51%	-44%	-51%
14	9/1/2018 17:00	9/5/2018 7:00	-8.91	-5.74E+07	41%	19%	-41%	-19%

Table A5

Error Values for Temperature-based AMM - Sewer MS0456

			Error		Absolute Percent Error		Percent Error	
Event Rank	Start	End	Peak Event (cfs)	Event Volume (cf)	Peak Event	Event Volume	Peak Event	Event Volume
1	9/27/2019 11:00	10/10/2019 2:00	-1.83	-9.92E+07	41%	31%	-41%	-31%
2	8/26/2018 10:00	9/1/2018 9:00	-9.22	-4.98E+07	59%	33%	-59%	-33%
3	5/17/2020 3:00	5/24/2020 12:00	5.30	1.45E+08	55%	72%	55%	72%
4	8/6/2021 1:00	8/13/2021 18:00	-1.04	3.19E+05	12%	0%	-12%	0%
5	9/11/2022 1:00	9/16/2022 10:00	1.84	3.87E+07	40%	80%	40%	80%
6	4/27/2020 9:00	5/6/2020 2:00	0.68	-6.37E+05	18%	2%	18%	-2%
7	6/18/2018 2:00	6/24/2018 7:00	0.37	5.34E+05	8%	1%	8%	1%
8	3/22/2022 9:00	3/28/2022 18:00	0.27	-1.60E+07	12%	25%	12%	-25%
9	9/29/2018 15:00	10/3/2018 23:00	-0.37	1.30E+07	10%	30%	-10%	30%
10	9/9/2019 3:00	9/16/2019 12:00	-1.53	1.57E+07	29%	24%	-29%	24%
11	12/9/2020 20:00	12/16/2020 6:00	-0.40	-1.20E+07	17%	31%	-17%	-31%
12	7/17/2019 21:00	7/24/2019 5:00	-0.74	1.05E+07	20%	24%	-20%	24%
13	7/5/2020 11:00	7/14/2020 8:00	-0.03	5.01E+06	1%	7%	-1%	7%
14	12/1/2018 7:00	12/6/2018 6:00	1.08	1.26E+07	50%	39%	50%	39%
15	8/20/2018 20:00	8/24/2018 3:00	0.28	8.06E+06	5%	39%	5%	39%

Table A6

Error Values for Two-level Model Using Milwaukee River - Sewer MS0456

			Error		Absolute Percent Error		Percent Error	
Event Rank	Start	End	Peak Event (cfs)	Event Volume (cf)	Peak Event	Event Volume	Peak Event	Event Volume
1	9/27/2019 11:00	10/10/2019 2:00	-0.98	-6.24E+07	22%	20%	-22%	-20%
2	8/26/2018 10:00	9/1/2018 9:00	-6.84	1.32E+07	43%	9%	-43%	9%
3	5/17/2020 3:00	5/24/2020 12:00	-0.72	9.18E+06	7%	5%	-7%	5%
4	8/6/2021 1:00	8/13/2021 18:00	2.27	6.00E+07	26%	40%	26%	40%
5	9/11/2022 1:00	9/16/2022 10:00	2.95	4.95E+07	64%	103%	64%	103%
6	4/27/2020 9:00	5/6/2020 2:00	-1.08	-7.28E+05	28%	3%	-28%	-3%
7	6/18/2018 2:00	6/24/2018 7:00	1.69	1.43E+07	37%	22%	37%	22%
8	3/22/2022 9:00	3/28/2022 18:00	-0.53	-3.36E+07	24%	53%	-24%	-53%
9	9/29/2018 15:00	10/3/2018 23:00	-1.25	-3.27E+06	34%	8%	-34%	-8%
10	9/9/2019 3:00	9/16/2019 12:00	-0.94	1.80E+07	18%	28%	-18%	28%
11	12/9/2020 20:00	12/16/2020 6:00	-1.03	-2.32E+07	44%	59%	-44%	-59%
12	7/17/2019 21:00	7/24/2019 5:00	-0.33	1.94E+07	9%	45%	-9%	45%
13	7/5/2020 11:00	7/14/2020 8:00	1.68	3.19E+07	44%	43%	44%	43%
14	12/1/2018 7:00	12/6/2018 6:00	-0.31	-1.14E+07	14%	36%	-14%	-36%
15	8/20/2018 20:00	8/24/2018 3:00	2.04	1.60E+07	37%	78%	37%	78%

Table A7

Error Values for Three-level Model Using Lincoln Creek - Sewer MS0456

			Error		Absolute Percent Error		Percent Error	
Event Rank	Start	End	Peak Event (cfs)	Event Volume (cf)	Peak Event	Event Volume	Peak Event	Event Volume
1	9/27/2019 11:00	10/10/2019 2:00	-1.80	-1.07E+08	41%	34%	-41%	-34%
2	8/26/2018 10:00	9/1/2018 9:00	-8.52	-3.13E+07	54%	21%	-54%	-21%
3	5/17/2020 3:00	5/24/2020 12:00	-3.46	-6.60E+07	36%	33%	-36%	-33%
4	8/6/2021 1:00	8/13/2021 18:00	0.16	3.32E+07	2%	22%	2%	22%
5	9/11/2022 1:00	9/16/2022 10:00	1.96	4.23E+07	43%	88%	43%	88%
6	4/27/2020 9:00	5/6/2020 2:00	-1.39	-8.52E+05	36%	3%	-36%	-3%
7	6/18/2018 2:00	6/24/2018 7:00	1.01	1.16E+07	22%	18%	22%	18%
8	3/22/2022 9:00	3/28/2022 18:00	-0.63	-3.48E+07	28%	55%	-28%	-55%
9	9/29/2018 15:00	10/3/2018 23:00	-1.22	-1.54E+06	34%	4%	-34%	-4%
10	9/9/2019 3:00	9/16/2019 12:00	-1.53	1.51E+07	29%	23%	-29%	23%
11	12/9/2020 20:00	12/16/2020 6:00	-1.08	-2.24E+07	46%	57%	-46%	-57%
12	7/17/2019 21:00	7/24/2019 5:00	-0.07	2.49E+07	2%	58%	-2%	58%
13	7/5/2020 11:00	7/14/2020 8:00	1.15	2.83E+07	30%	39%	30%	39%
14	12/1/2018 7:00	12/6/2018 6:00	-0.45	-1.04E+07	21%	32%	-21%	-32%
15	8/20/2018 20:00	8/24/2018 3:00	1.54	1.60E+07	28%	78%	28%	78%

Table A8

Error Values for Two-level Model Using Lincoln Creek - Sewer MS0456

			Error		Absolute Percent Error		Percent Error	
Event Rank	Start	End	Peak Event (cfs)	Event Volume (cf)	Peak Event	Event Volume	Peak Event	Event Volume
1	9/27/2019 11:00	10/10/2019 2:00	-1.38	-106820948.9	31%	34%	-31%	-34%
2	8/26/2018 10:00	9/1/2018 9:00	-6.09	4560682.592	39%	3%	-39%	3%
3	5/17/2020 3:00	5/24/2020 12:00	-1.26	-23317294.98	13%	12%	-13%	-12%
4	8/6/2021 1:00	8/13/2021 18:00	1.72	52111852.44	20%	35%	20%	35%
5	9/11/2022 1:00	9/16/2022 10:00	3.31	47094331.76	72%	97%	72%	97%
6	4/27/2020 9:00	5/6/2020 2:00	-1.45	-868803.6829	38%	3%	-38%	-3%
7	6/18/2018 2:00	6/24/2018 7:00	2.15	26039894.87	48%	39%	48%	39%
8	3/22/2022 9:00	3/28/2022 18:00	-0.85	-39650213.74	38%	62%	-38%	-62%
9	9/29/2018 15:00	10/3/2018 23:00	-1.05	-3440235.626	29%	8%	-29%	-8%
10	9/9/2019 3:00	9/16/2019 12:00	-0.87	13963552.55	17%	22%	-17%	22%
11	12/9/2020 20:00	12/16/2020 6:00	-1.23	-25185950.2	53%	64%	-53%	-64%
12	7/17/2019 21:00	7/24/2019 5:00	0.10	20525514.18	3%	47%	3%	47%
13	7/5/2020 11:00	7/14/2020 8:00	1.47	24471476.05	39%	33%	39%	33%
14	12/1/2018 7:00	12/6/2018 6:00	-0.75	-14791230.1	35%	46%	-35%	-46%
15	8/20/2018 20:00	8/24/2018 3:00	1.84	14789976.18	33%	72%	33%	72%

Appendix B: ChatGPT Raw Output

```
% Create an Excel application object
ExcelApp = actxserver('Excel.Application');

% Set Excel to be visible (optional)
ExcelApp.Visible = 1;

% Open the Excel file (replace 'your_file.xlsx' with the actual file path)
Workbook = ExcelApp.Workbooks.Open('C:\your_file_path\your_file.xlsx');

% Get a reference to the first sheet in the workbook
Sheet1 = Workbook.Sheets.Item(1);

% Set the value of cell A7
Sheet1.Range('A7').Value = 15.3;

% Recalculate
ExcelApp.Calculate;

% Retrieve the value from cell D23 and store it in a MATLAB variable
result = Sheet1.Range('D23').Value;

% Close the workbook and save changes
```

```
Workbook.Close(true);

% Quit Excel
ExcelApp.Quit;

% Release the COM objects
Workbook.release;
ExcelApp.release;

% Display the result
disp(['The value in cell D23 is: ', num2str(result)]);
```

Replace 'C:\your_file_path\your_file.xlsx' with the correct path to your Excel file. This code assumes that the Excel file contains at least one worksheet and that you are interested in interacting with the first sheet.

Civil Engineering

Capstone Report Approval Form

Master of Science in Civil Engineering – MSCVE

Milwaukee School of Engineering

This capstone report, titled "Using Stream Gages to Represent Antecedent Moisture Conditions in the Antecedent Moisture Model," submitted by the student Alex R. Luedke, has been approved by the following committee:

Faculty Advisor: _____ Date: _____

Dr. William Gonwa, Ph.D.

Faculty Member: _____ Date: _____

Dr. Eric Durant, Ph.D.

Faculty Member: _____ Date: _____

Dr. Anne Alexander, Ph.D.